The Astrophysical Journal, 715:1419–1437, 2010 June 1 doi:10.1088/0004-637X/715/2/1419

THE ADVANCED CAMERA FOR SURVEYS FORNAX CLUSTER SURVEY. VII. HALF-LIGHT RADII OF GLOBULAR CLUSTERS IN EARLY-TYPE GALAXIES

Karen L. Masters[1,2], Andrés Jordán[2,3], Patrick Côté[4], Laura Ferrarese[4], John P. Blakeslee[4], Leopoldo Infante[3], Eric W. Peng[5,6], Simona Mei[7], and Michael J. West[8]

[1] Institute for Cosmology and Gravitation, University of Portsmouth, Dennis Sciama Building, Burnaby Road, Portsmouth, PO1 3FX, UK; karen.masters@port.ac.uk
[2] Harvard-Smithsonian Center for Astrophysics, 60 Garden Street, Cambridge, MA 02138, USA
[3] Departamento de Astronomía y Astrofísica, Pontificia Universidad Católica de Chile, 7820436 Macul, Santiago, Chile
[4] Herzberg Institute of Astrophysics, Victoria, BC V9E 2E7, Canada
[5] Department of Astronomy, Peking University, Beijing 100871, China
[6] Kavli Institute for Astronomy and Astrophysics, Peking University, Beijing 100871, China
[7] GEPI, Observatoire de Paris, Section de Meudon, 5 Place Jules Janssen, 92195 Meudon Cedex, France
[8] ESO, Alonso de Córdova 3107, Vitacura, Santiago, Chile

Received 2009 August 28; accepted 2010 February 25; published 2010 May 12

ABSTRACT

We measure the half-light radii of globular clusters (GCs) in 43 galaxies from the Advanced Camera for Surveys (ACS) Fornax Cluster Survey. We use these data to extend previous work in which the environmental dependencies of the half-light radii of GCs in early-type galaxies in the ACS Virgo Cluster Survey were studied, and a corrected mean half-light radius (corrected for the observed environmental trends) was suggested as a reliable distance indicator. This work both increases the sample size for the study of the environmental dependencies, and adds leverage to the study of the corrected half-light radius as a possible distance indicator (since Fornax lies at a larger distance than the Virgo cluster). We study the environmental dependencies of the size of GCs using both a Principal Component Analysis as well as two-dimensional scaling relations. We largely confirm the environmental dependencies shown in Jordán et al., but find evidence that there is a residual correlation in the mean half-light radius of GC systems with galaxy magnitude, and subtle differences in the other correlations—so there may not be a universal correction for the half-light radii of lower luminosity galaxy GC systems. The main factor determining the size of a GC in an early-type galaxy is the GC color. Red GCs have $\langle r_h \rangle = 2.8 \pm 0.3$ pc, while blue GCs have $\langle r_h \rangle = 3.4 \pm 0.3$ pc. We show that for bright early-type galaxies ($M_B < -19$ mag), the uncorrected mean half-light radius of the GC system is by itself an excellent distance indicator (with error ∼11%), having the potential to reach cosmologically interesting distances in the era of high angular resolution adaptive optics on large optical telescopes.

Key words: galaxies: elliptical and lenticular, cD – galaxies: star clusters: general – globular clusters: general

Online-only material: color figures

1. INTRODUCTION

The launch of the *Hubble Space Telescope* (*HST*) revolutionized areas of astronomy which push the limits of high resolution imaging. One area which benefited has been the study of the half-light radii, r_h, of globular clusters (GCs). A typical GC has a half-light radius of a few parsecs. Ground-based imaging (before the era of adaptive optics) could resolve such objects only in galaxies in the Local Group (LG). This limited the statistics and confined the study to the GC systems in dwarf and late-type galaxies (e.g., the sample in Forbes et al. 2000). *HST* opened the study to GC systems in galaxies out to ∼30 Mpc, encompassing large numbers of all types of galaxies and including both the Virgo and Fornax clusters (at $\sim 16.5 \pm 1.1$ Mpc from Mei et al. 2007 and 20.0 ± 1.4 Mpc from Blakeslee et al. 2009, respectively).

Interest in the half-light radius of GCs results both from the constraints they provide on the formation and evolution of GCs and also their possible use as a distance indicator, which dates back to an initial suggestion by Shapley & Sawyer (1927). The half-light radii of GCs, rather remarkably, are almost independent of GC mass (McLaughlin 2000; Jordán et al. 2005; Barmby et al. 2007; McLaughlin et al. 2008; Harris 2009; Harris et al. 2009b), at least to $\sim 10^6\ M_\odot$ (Haşegan et al. 2005; Murray 2009). In simulations, they have been shown to be fairly constant as the GCs evolve (Spitzer & Thuan 1972; Lightman & Shapiro 1978; Murphy et al. 1990; Aarseth & Heggie 1998), and may in fact trace the characteristic sizes of the proto-GC cloud (Murray & Lin 1992; Harris et al. 2009b). In the Milky Way (MW), it has long been known that r_h increases systematically with galactocentric distance, although *HST* studies (Kundu & Whitmore 2001; Jordán et al. 2005; Harris 2009) have shown that in early types, r_h is much closer to being constant with galactocentric radius.

In this paper, we extend the work of Jordán et al. (2005, hereafter J05) which used Advanced Camera for Surveys (ACS) data on GCs in Virgo cluster galaxies (from the ACS Virgo Cluster Survey, ACSVCS; Côté et al. 2004) to study the environmental impacts on the r_h of GCs and calibrated a corrected mean half-light radius (i.e., corrected for the observed environmental trends) as a distance indicator. We add to this study similar data from the ACS Fornax Cluster Survey (ACSFCS; Jordán et al. 2007a). This adds 43 galaxies to the sample, and also extends the lever arm for calibration of the corrected mean half-light radius as a distance indicator since the Fornax cluster is at a larger distance than the Virgo cluster.

Other recent works have studied the half-light radius of GCs, extending both the total number and range of morphologies and environments studied. GC sizes in M31 and NGC 5128 were studied with emphasis on the fundamental plane of GCs by

Barmby et al. (2007) and McLaughlin et al. (2008), respectively. Barmby et al. (2007) show (using data for M31, NGC 5128, the MW, the Magellanic Clouds, and the Fornax dwarf spheroidal) that old GCs appear to have near-universal structural properties. Measurements of GC sizes in late-type galaxies beyond the LG include the Sombrero galaxy (Spitler et al. 2006; Harris et al. 2009b), NGC 891 (Harris et al. 2009a), and NGC 5190 (Forbes et al. 2010). Extremes in host galaxy luminosity are encompassed by the work on dwarf galaxies by Georgiev et al. (2009) and the study of six giant ellipticals of Harris (2009). DeGraaff et al. (2007) studied the SB0 galaxy NGC 1533 in the Dorado group. At the limit of what can be currently done from the ground is the work of Gómez & Woodley (2007), who used IMACS at the Magellan telescopes to study GC sizes in NGC 5128. As we will comment below, these works extend many of the results on GC sizes we have obtained using the ACSVCS and ACSFCS to different host galaxy morphologies and environments. All in all, the structural properties of GCs seem to share many near-universal properties across galaxy morphology and luminosity, but some differences seem to exist as well.

The paper is organized as follows. In Section 2, we describe the data. In Section 3, we present the distributions of r_h in Fornax early-type galaxies. In Section 4, we describe the possible environmental dependencies which we explore with a principle components analysis (PCA) in the Appendix and traditional two-dimensional (2D) trends in Section 5. In Section 6, we show the final corrections which are discussed in Section 7, both as tracers of the GC formation and evolution and for implications on the use of a corrected mean half-light radius as a distance indicator. Section 8 presents a summary of our conclusions.

2. OBSERVATIONS

As part of the ACSFCS (Jordán et al. 2007a), a sample of 43 early-type galaxies in the Fornax cluster were observed in the F475W (≈ Sloan g) and F850LP (≈ Sloan z) filters. The ACSFCS sample was constructed from the Fornax Cluster Catalog (FCC; Ferguson 1989) as described in Jordán et al. (2007a) using the FCC galaxy morphologies. Half-light radii are measured for all GC candidates using the procedure explained in detail in J05 which fits a point-spread function (PSF)-convolved King model to the GCs in both bands. The final result quoted here is the average of the measurement in both bands. The measurement of r_h is obviously challenging in the cases for which the GCs are only marginally resolved. J05 show in their Appendix A that their code recovers r_h with no bias to $r_h \sim 0.3$ pixels (which is 0.″015 or ∼1.2 pc at the distance of Virgo; ∼1.4 pc at the distance of Fornax) under typical observing conditions, assuming the PSF model is correct and that GCs are correctly modeled by a King profile. As discussed in J05, the systematic uncertainties due to the modeling of the PSF are of the order of 0.05 WFC pixels (2.5 mas), or ∼0.25 pc at the distance of Fornax. The level of systematic uncertainties was estimated in J05 by comparing the measurements done independently in each of the two available bands. This estimate of the level of systematic uncertainty agrees well with independent estimates of this quantity given by Harris (2009), who uses different data sets and code to measure r_h with ACS/WFC, and with those derived from a comparison of r_h measurements done using two different ACS/WFC data sets of M87 using the same code we use here (Peng et al. 2009). Thus, the r_h we measure, and in particular their potential use as distance indicator, are not tied to our particular observational setup beyond possible systematic effects at the level of a few milliarcseconds.[9]

Table 1
Basic Information on Galaxies and GC Systems from ACSFCS Sample

Name	B mag	N_{GC}	$\langle r_h \rangle$ (arcsec)	Other Name
FCC 21	9.40	232	0.040 ± 0.002	NGC 1316
FCC 213	10.60	698	0.027 ± 0.001	NGC 1399
FCC 219	10.90	220	0.029 ± 0.001	NGC 1404
NGC 1340	11.27	137	0.030 ± 0.002	NGC 1344
FCC 167	11.30	266	0.032 ± 0.001	NGC 1380
FCC 276	11.80	232	0.025 ± 0.001	NGC 1427
FCC 147	11.90	201	0.028 ± 0.001	NGC 1374
IC 2006	12.21	89	0.034 ± 0.002	ESO 359-G7
FCC 184	12.30	216	0.030 ± 0.001	NGC 1387
FCC 83	12.30	173	0.032 ± 0.001	NGC 1351
FCC 63	12.70	142	0.034 ± 0.002	NGC 1339
FCC 193	12.80	23	0.046 ± 0.006	NGC 1389
FCC 170	13.00	30	0.030 ± 0.004	NGC 1381
FCC 153	13.00	28	0.037 ± 0.004	IC 1963
FCC 177	13.20	47	0.038 ± 0.003	NGC 1380A
FCC 47	13.30	184	0.032 ± 0.001	NGC 1336
FCC 310	13.50	18	0.028 ± 0.004	NGC 1460
FCC 43	13.50	15	0.036 ± 0.006	IC 1919
FCC 190	13.50	103	0.041 ± 0.002	NGC 1380B
FCC 148	13.60	13	0.035 ± 0.007	NGC 1375
FCC 249	13.60	102	0.036 ± 0.002	NGC 1419
FCC 255	13.70	57	0.035 ± 0.003	ESO 358-G50
FCC 277	13.80	17	0.034 ± 0.003	NGC 1428
FCC 55	13.90	12	0.034 ± 0.004	ESO 358-G06
FCC 152	14.10	5	0.050 ± 0.021	ESO 358-G25
FCC 143	14.30	33	0.033 ± 0.004	NGC 1373
FCC 95	14.60	13	0.049 ± 0.011	MCG-06-08-025
FCC 136	14.80	13	0.045 ± 0.004	MCG-06-08-027
FCC 182	14.90	22	0.039 ± 0.005	MCG-06-09-008
FCC 204	14.90	7	0.050 ± 0.020	ESO 358-G43
FCC 90	15.00	8	0.040 ± 0.010	MCG-06-08-024
FCC 26	15.00	14	0.041 ± 0.008	ESO 357-G25
FCC 106	15.10	5	0.042 ± 0.020	···
FCC 324	15.30	7	0.036 ± 0.007	ESO 358-G66
FCC 100	15.50	9	0.044 ± 0.013	···
FCC 203	15.50	10	0.046 ± 0.007	ESO 358-G42
FCC 303	15.50	10	0.051 ± 0.009	MCG-06-09-028

We follow J05 in the construction of GC catalogs in each galaxy. The procedure is described in detail in Jordán et al. (2009) and summarized in J05, so we only list here in brief the cuts made. GCs are selected using the maximum likelihood estimated probability (Jordán et al. 2009) of $p_{GC} \geqslant 0.5$, z-band magnitude, $z \leqslant 23.35$ mag, and colors, $0.6 \leqslant (g - z) \leqslant 1.7$ mag. This selection on magnitude is roughly equivalent to the Virgo cut of $z \leqslant 22.9$ mag at the expected turnover of the GC luminosity function (GCLF) shifted to the greater distance of Fornax. Contamination and reliability cuts result in a size range of $r_h = 0.75$–10 pc for objects which can be reliably identified as GCs.

The ACSFCS measures distances using the surface brightness fluctuation (SBF) method for all 43 galaxies in the sample (Blakeslee et al. 2009), therefore allowing study of the *physical* half-light radii of all GCs. We restrict the sample to galaxies with five or more GCs (also removing FCC 202 whose GC system is overwhelmed by its much larger companion, FCC 213). This leaves a final sample of 37 Fornax cluster galaxies. Table 1 lists

[9] One caveat is that the effects of mass segregation can make the measured r_h wavelength dependent, with an expected variation of ∼5% between the V- and I-bands (see, e.g., Madrid et al. 2009).

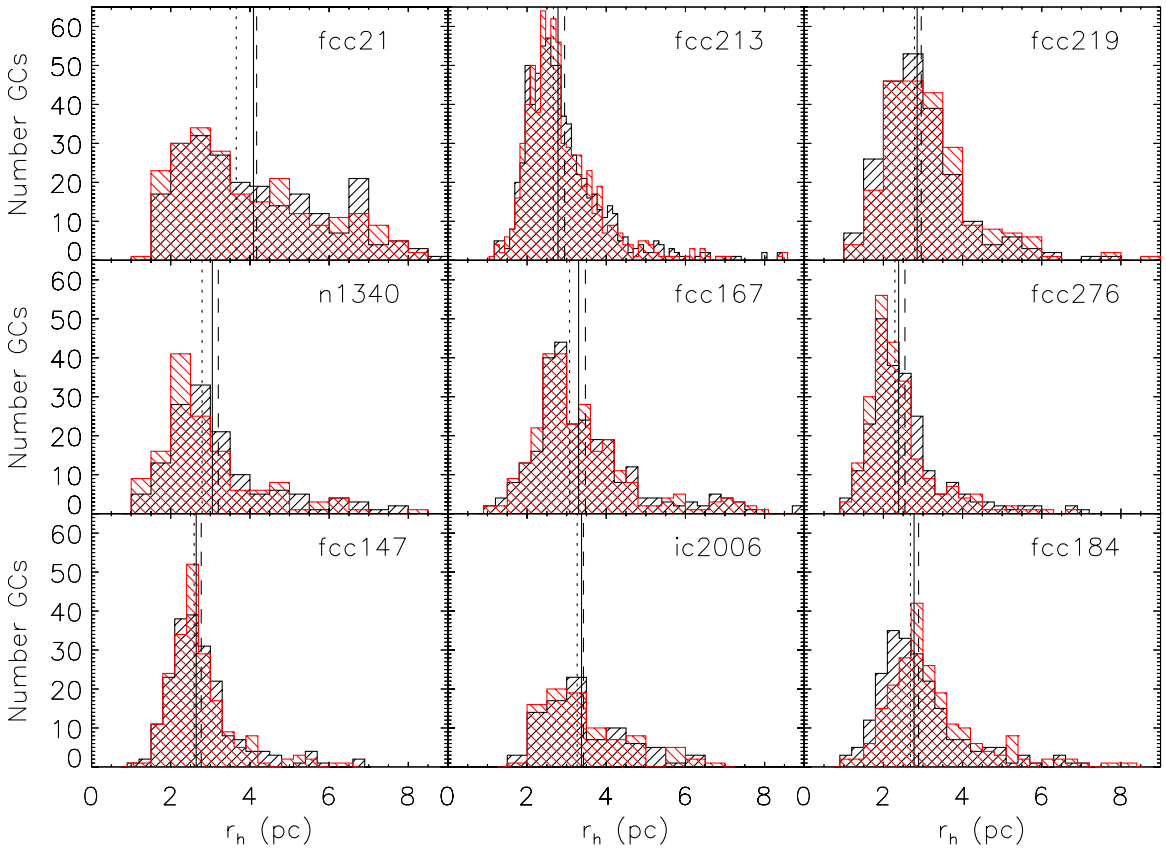

Figure 1. Distribution of uncorrected r_h, and corrected $\hat{r}_h$ values (in pc) for the nine most luminous galaxies in Fornax. Uncorrected values are shown by the forward diagonal hashed histogram, corrected by the backward diagonal (red) hashed histogram. For the uncorrected values, the solid vertical line shows the biweight location estimation of the mean, the dashed line is the normal mean, and the dotted line is the median value.

(A color version of this figure is available in the online journal.)

Table 2
Symbols Used to Describe the Half-light Radii of GCs

Symbol	Description
r_h	Measured half-light radius for an individual GC
$\langle r_h \rangle$	Average (usually biweight mean) of all measures of r_h in a given galaxy
r'_h	r_h corrected for dependence on local galaxy surface brightness (see Section 5.2, Equation (1))
$\langle r'_h \rangle$	Average of r'_h
r''_h	r'_h corrected for dependence of $\langle r'_h \rangle$ on galaxy color (see Section 5.3, Equations (5) and (6))
$\langle r''_h \rangle$	Average of r''_h
$\hat{r}_h$	r''_h corrected for dependence on GC color (see Section 5.4)
$\langle \hat{r}_h \rangle$	Average of $\hat{r}_h$
$\hat{r}'_h$	$\hat{r}_h$ corrected for a residual dependence of $\langle r'_h \rangle$ on galaxy magnitude (see Sections 5.3 and 6)
$\langle \hat{r}'_h \rangle$	Average of $\hat{r}'_h$

these galaxies showing (1) FCC number, (2) *B*-band magnitude from Ferguson (1989), (3) number of GCs, (4) average value of r_h calculated using a biweight location estimator, and (5) alternative names for the galaxies.

In some sections, we also consider the sample of GCs in Virgo cluster galaxies discussed in J05. Because of slight changes in the program which calculated the GC probabilities, p_{GC}, we find a slightly different sample than is used in J05; in general, we find that each galaxy has a few more GCs than were used in J05. We also add the galaxies VCC21, VCC1833, VCC1440, and VCC1075 which have very small GC systems and previously were just below the cutoff of $N_{GC} = 5$ used in J05.

3. DISTRIBUTION OF r_h IN FORNAX CLUSTER GALAXIES

In this paper, we will use several different symbols to describe the half-light radius of GCs. We start this section by providing a reference table of these symbols. Table 2 lists all the symbols used along with a brief description of what they represent and a reference to the section of the paper that defines it (if appropriate).

The distribution of both raw r_h, and corrected ($\hat{r}_h$) values for all GCs in the system is shown for the nine most luminous Fornax cluster galaxies in Figure 1. In those figures, the solid vertical line shows the biweight location estimation of the mean

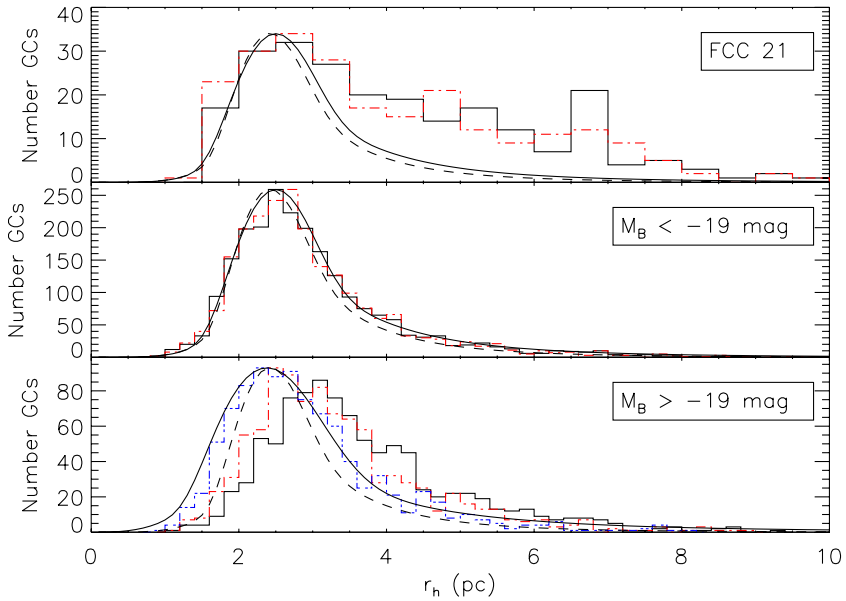

Figure 2. Distribution of uncorrected (r_h in black solid histogram) and corrected ($\hat{r}_h$ in red, dot-dashed histogram) values (in pc) for (1) FCC 21, (2) all other bright Fornax galaxies ($M_B < -19$ mag), and (3) fainter Fornax cluster early types ($M_B > -19$ mag). Also shown for the fainter galaxies is the "extra" corrected, $\hat{r}'_h$ (in blue dot-dot-dot-dashed histogram). The dashed curve shows the function fitted in J05 to the distribution of $\hat{r}_h$ from ACSVCS with its peak normalized to the peak of the observed distribution, while the solid line in the two upper panels are our best fit of the same function to the bright Fornax cluster galaxy GC systems, and in the lower panel it is the fit to the fainter Fornax cluster galaxy GC systems.

(A color version of this figure is available in the online journal.)

of r_h, the dashed line is the normal mean, and the dotted line is the median value. The distribution of r_h in all cases is quite far from normal with a long tail to large values of r_h as was previously found by J05 for GC systems in the ACSVCS. The median value of r_h is therefore always smaller than the other estimates of the mean. In addition to galaxies in the LG, Virgo, and Fornax, this form of the GC size distribution has now been observed in galaxies with a wide range of morphologies and luminosities (Georgiev et al. 2009; Harris 2009; Harris et al. 2009b).

FCC 21 (or Fornax A) shows a rather peculiar distribution of GC half-light radii, with a much larger than normal number of extended GCs. This skews the average r_h for FCC 21 to a much larger value than expected. Note that FCC 21 is the most luminous early-type galaxy in the Fornax cluster and shows unmistakable evidence for a recent merger (Schweizer 1980; Goudfrooij 2001) which may account for this odd distribution of GC sizes.[10] We do not exclude the GC system of FCC21 from the sample at this time, but will pay close attention to it in what follows.

We show in Figure 2 the grouped GC systems of FCC 21 alone, the remaining bright galaxies ($M_B < -19$ mag, excluding FCC21), and the dimmer galaxies ($M_B > -19$ mag), with the fitting function whose parameters are given in Equation (27) of J05 overlaid (dashed curve). The shape of the r_h distribution for the fainter galaxies is very similar to the luminous galaxies, but the mean is shifted to a higher value. We also show here the distribution of corrected $\hat{r}_h$ values (red, dot-dashed histogram) and for the dimmer galaxies the "extra" corrected, $\hat{r}'_h$ values (blue, dot-dot-dot-dashed histogram) as discussed in Section 7. We perform a maximum likelihood fit of the function described in Equations (24) and (25) of J05 to the histograms of $\hat{r}_h$ for the bright galaxies and $\hat{r}'_h$ for the dimmer galaxies finding best-fit values of the parameters ($\tilde{\mu}$, $\tilde{\beta}_1$, $\tilde{\beta}_2$, and $\tilde{f}$) of (2.65, 0.32, 0.18, 0.70) and (2.64, 0.34, 0.25, 0.61) within a few σ of the quoted dispersion on these values found from fits to a range of ACSVCS galaxies in J05 (whose errors describing the range of fits in Virgo cluster galaxies of different colors would therefore be reasonable estimates here too). These functional fits are overlaid in Figure 2 as the solid curves. It is clear that the fit to the distribution of GC sizes in the bright Fornax cluster galaxies is very similar to that found for Virgo galaxies by J05, further demonstrating the universality of the distribution of GC sizes in early-type galaxies, especially the most luminous ones.

4. FACTORS WHICH MIGHT AFFECT GC SIZE

It is plausible that many factors may influence the size of a GC. This could include properties of the GC themselves (such as mass, metallicity, or age) as well as external factors related both to the local environment at the position of the GC, as well as differences in the type or size of galaxy in which the GC formed and evolved. Following J05, we separate possible dependencies of the GC half-light radius into three categories.

1. *Internal Factors.* In this category, we consider trends of the half-light radius with properties of the GCs themselves. We use the z-band absolute magnitude (as a proxy for GC mass) and the $(g - z)$ colors which correlate with GC metallicity and age. Both quantities are measured directly from the ACS imaging.
2. *Local Factors.* In this category, we consider trends of r_h with tracers of the local environment of the GC. We consider the GC's position in its host galaxy, using the galactic radius scaled to the effective radius of the host galaxy (r_p/r_e) and also the local surface brightness, μ_z, and local color $\mu_g - \mu_z$

[10] Recently, Da Costa et al. (2009) suggested that here may be two modes of star formation in dwarf galaxies, a "normal" mode with $r_h \sim 3$ pc and an "extended" mode with $r_h \sim 10$ pc. This "extended" mode, if real, could be potentially related to the excess of large GCs we find in FCC 21.

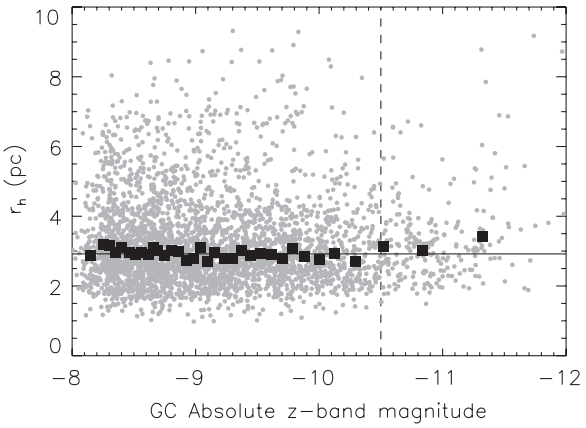

Figure 3. Half-light radii (r_h) vs. z-band absolute magnitude of GCs in early-type galaxies in the Fornax cluster. Overlaid are the median values in bins of 100 GCs. The horizontal line shows the median value for the whole sample of 2.94 pc. We indicate the z-band magnitude corresponding to $M = 2 \times 10^6\ M_\odot$ (assuming $M/L_z \sim 1.5$ in solar units; Jordán et al. 2007b) where a mass–radius relation has previously been shown to emerge.

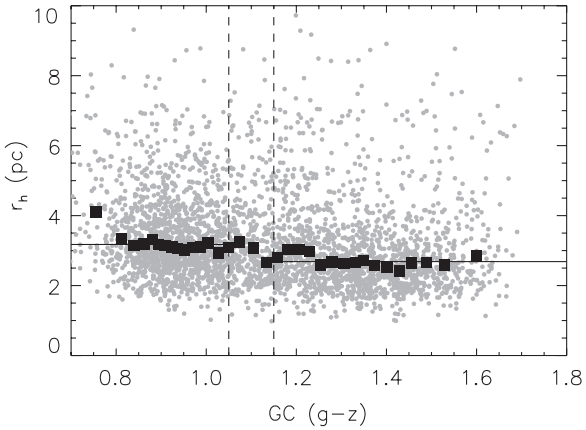

Figure 4. Half-light radii (r_h) vs. color ($g-z$) of GCs in early-type galaxies in the Fornax cluster. Overlaid are the median values in bins of 100 GCs. The vertical dashed lines show our color cuts for blue GCs ($g - z < 1.05$) and red GCs ($g - z > 1.15$). The horizontal solid lines show the mean r_h values for the blue and red GCs, respectively.

at the position of the GC. The derivation of these quantities from ACS images are described in Ferrarese et al. (2006).

3. *Global Factors.* In this category, we consider trends of r_h with global properties of the host galaxy. For this, we consider the absolute B-band magnitudes, M_B (from the RC3, de Vaucouleurs et al. 1991), as well as the $(g-z)$ color and the average z-band surface brightness both measured within the effective radius, r_e from the ACS images. The galaxies FCC 167 and FCC 26 have very poor fits to their ACS data due to the presence of a massive dust disk and a region of star formation, the inner region of FCC 167 and FCC 26, respectively. In the case of FCC 167, no effective radius could be measured (so we take the one in the RC3), and in both cases the global colors are difficult to define. For these galaxies, we use the average color from the areas of the galaxies used for SBF measurements in Blakeslee et al. (2009).

As is discussed in J05, there is a significant interdependency between many of these parameters: for example, it is well known that a galaxy's total magnitude correlates with color, and the colors of the GCs in a galaxy are also correlated with both the galaxy's total magnitude and color. This makes the problem an ideal candidate for a PCA to look for the primary correlations. Such an analysis is performed in the Appendix. We will also consider the traditional 2D scaling relations below in Section 5.

5. TRENDS BETWEEN VARIABLES

In this section, we separately consider trends between variables, using traditional 2D plots and constructing best-fit relations. In the Appendix, we describe a PCA which as discussed in Section 4 above is particularly useful for learning about the shape of the correlations between many different variables when significant intercorrelations are expected. However, it is still simpler to interpret the traditional 2D trends between variables (plotting one as a function of the other), and by doing this successively with different factors the interdependencies can also be traced. The PCA in the Appendix has given us an idea of the shape of the trends we expect to see and which relations we expect to be important and unimportant (showing that the variability in r_h can be well described by one factor from each of the internal, local, and global categories we define in Section 4); however, we will consider all possible factors again in what follows.

5.1. Internal Factors

In this section, we consider how properties of the GCs themselves might affect the observed sizes of the GCs.

It has been seen in previous *HST* studies (Kundu & Whitmore 2001; J05; Barmby et al. 2007; McLaughlin et al. 2008; Harris 2009; Harris et al. 2009b; Madrid et al. 2009) that the size of GCs is roughly independent of their mass and luminosity at least for GCs with masses below $M = 2 \times 10^6\ M_\odot$ (Haşegan et al. 2005; Murray 2009). As expected, we confirm this property with GCs in Fornax cluster galaxies—we see no significant correlation of r_h with the luminosity of the GCs (see Figure 3). We indicate the z-band magnitude corresponding to $M = 2 \times 10^6 M_\odot$ (assuming $M/L_z \sim 1.5$ in solar units, Jordán et al. 2007b); at brighter magnitudes (larger masses) than this there is a hint of an upturn in the relation of r_h and magnitude. Spitler et al. (2006) suggest that in the Sombrero galaxy, an Sa/S0 central galaxy in a small group, there is a statistically significant trend of the sizes of the red GCs with absolute magnitude. Splitting the GCs in our sample into red and blue, however, we see no significant differences in the trend with magnitude. Both subsamples of GCs in early-type Fornax cluster galaxies are consistent with having no size–luminosity relation.

As has also been seen in previous *HST* studies of GCs in bright ellipticals (e.g., Kundu et al. 1999; Puzia et al. 1999; Larsen et al. 2001; J05; Madrid et al. 2009; Harris 2009), we find a clear correlation of r_h with GC color, with bluer GCs having larger half-light radii (see Figure 4). We follow J05 in restricting the sample in color in order to study other correlations, considering blue GCs ($(g - z) < 1.05$) and red GCs ($(g - z) > 1.15$) separately in what follows, and returning to the issue of the color dependence later. The reason for separating the GCs by color is that many of the properties of GCs are correlated with GC color, making it hard to separate the dependencies on each variable. For example, the dependence of $\langle r_h \rangle$ on GC color will affect the measured dependence of $\langle r_h \rangle$ with galactocentric radius through the changing ratio of red to blue GCs with this quantity (see Section 3 in J05 for more examples); by restricting the sample by color, we alleviate these problems. These color cuts correspond roughly to cuts in metallicity of [Fe/H] $\lesssim -0.8$

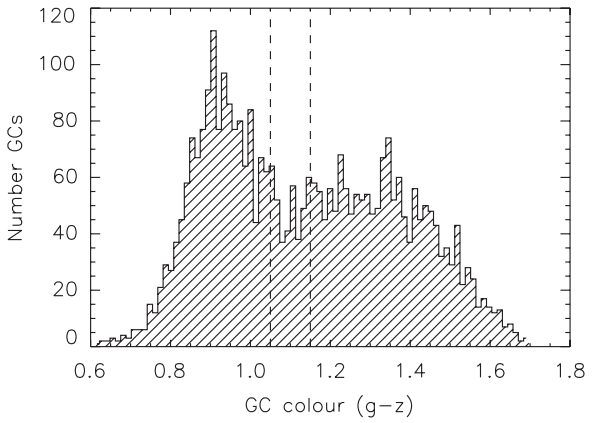

Figure 5. Distribution of GC colors for the combined sample of Fornax cluster galaxy GCs. The vertical solid lines show our color cuts for blue GCs ($g-z<1.05$) and red GCs ($g-z>1.15$).

(blue) and [Fe/H] $\gtrsim -0.65$ (red), where we have used the empirical relation between [Fe/H] and $(g-z)$ presented in Peng et al. (2006) derived using MW GC data to transform $(g-z)$ color to [Fe/H]. Within each of these color bins (shown in Figures 4 and 5), there is little evidence for a trend of r_h with color. This is especially true for the red GCs—there may still be a slight trend for the bluest of the blue GCs to have large values of r_h than the mean. The median value of r_h for blue GCs is 3.17 pc, and for red GCs it is 2.69 pc; using a biweight mean, we find $\langle r_h\rangle_{\rm blue} = 3.36\pm0.03$ pc ($\sigma = 1.1$ pc) and $\langle r_h\rangle_{\rm red} = 2.83\pm0.02$ pc ($\sigma = 1.0$ pc). The systematic error on both these measurements at the distance of Fornax is ∼0.25 pc (see J05; Section 2).

Possible explanations for this observed correlation between r_h and color are given by projection effects combined with a correlation between r_h and galactocentric distance similar to that of the MW (Larsen & Brodie 2003), the combined effects of mass segregation, and the dependence of stellar lifetimes on metallicity (Jordán 2004) or different conditions at formation (Harris 2009).

5.2. Local Factors

Here, we will look at how the local environment of a GC at the position it is found in its galaxy might affect the observed size of the GC. Using the sample of GCs separated into a blue subsample and a red subsample, we now look for correlations with projected galactocentric radius, r_p, local galaxy surface brightness, μ_z, and local galaxy color, $\mu_g-\mu_z$. Obviously, these factors are strongly correlated. In particular, we expect $\mu \propto \log[F(r_p)]$, where F is some function describing the shape of the surface brightness profile of a given galaxy. This does not mean that descriptions in the two different variables are equivalent since the function F can be quite complicated; however, there will be significant correlation between the two. In ellipticals, it is also generally the case that there is a color gradient with a bluer mean color in the outskirts of the galaxy than is observed in the central regions (as seen in ACSVCS data by Ferrarese et al. 2006). Ultimately, we will follow J05 in choosing μ_z as the most reliable independent variable, however, to begin with we will consider correlations with all three factors.

In order to place all GC systems on the same scale, we normalize their galactocentric radii using the effective radii of the galaxy, r_e as measured from the ACS images (L. Ferrarese et al. 2010, in preparation; note that in FCC 167, heavy dust obscuration prevented fitting the ACS image—in this case, r_e is taken from the RC3). Figure 6 shows half-light radius, r_h versus projected galactocentric distance, r_p/r_e for the blue GCs in the nine brightest early-type Fornax cluster galaxies. In the two brightest ACSFCS galaxies (FCC 21 and FCC 213), GCs are only traced to a couple of effective radii, but the vast majority of ACSFCS galaxies have GC data out to at least $5r_e$, with the maximum value in the sample being $14r_e$ (for FCC 249, $r_e = 7\farcs6$).

A small trend is visible in most galaxies, with GCs at larger galactocentric radii having, on average, slightly larger half-light radii. We fit simple linear relations of the form $\log(r_h) = a_r + b_r\log(r_p/r_e)$ to the data in all Fornax cluster galaxies, then take a weighted average of these results finding $b_r = 0.029\pm0.016$. There is no significant trend of the slope of the relation with the extent of the observed GC system ($r_{p,\rm max}/r_e$) suggesting that we are not hiding a stronger relation by being dominated by GCs in bright galaxies for which the radial extent of observed GCs is small. In contrast to the findings of Spitler et al. (2006) for the Sombrero galaxy, we do not find a significantly stronger trend with the red GC population than the blue ones, measuring $b_{r,\rm red} = 0.041\pm0.026$, which is the same as the trend of the blue GCs to within the 1σ errors. We do the same fits for $\log r_h$ versus μ_z (see Figure 7) finding in this case $b_\mu = 0.006\pm0.003$ from a weighted mean of the fits for each galaxy. These results are similar to, but a bit flatter (less significant) than the relations found in J05 for GCs in Virgo cluster galaxies of $b_r = 0.07\pm0.01$ and $b_\mu = 0.016\pm0.003$. We do this same fit again for the Virgo sample, and find $b_\mu = 0.011\pm0.003$ (the slight difference being due to slight changes in the sample and fitting methods). A combination of GC systems in Fornax and Virgo galaxies gives $b_\mu = 0.008\pm0.002$.

We also consider the radii of the blue GC versus the local color of the galaxy $(\mu_g-\mu_z)$, which is shown in Figure 8. The outer parts of the early-type galaxies in Fornax are all bluer than the inner parts. This corresponds to a trend with GC half-light radius such that those with redder local galaxy colors are, on average, slightly smaller. However, a fit of the form $\log(r_h) = a_c + b_c(\mu_g-\mu_z)$ results in a mean value of $b_c = -0.012\pm0.013$—a negligible trend.

These results come from the blue GCs only, but no significant differences are seen if just the red GCs are considered. The exclusion of GCs in the peculiar GC system of FCC 21 (= NGC 1316, Fornax A) which are currently included, also has little impact on the final results here.

We now correct the half-light radii of the GCs to what is expected for a GC with an underlying surface brightness of 21 mag arcsec^{-2}. Since we want a global correction for all GCs, we will use the slope of trend fit to both Fornax and Virgo cluster early-type GC systems together of

$$r_h' \equiv r_h 10^{-0.008(\mu_z-21)}. \quad (1)$$

There is evidence however that the trend is slightly stronger in the Virgo galaxies, and slightly weaker (possibly zero) in the Fornax galaxies. This is also a weaker trend than in J05, who used $r_h' \equiv r_h 10^{-0.016(\mu_z-21)}$.

5.3. Global Factors

We now look for correlations of the GC half-light radius with global properties of the host galaxy, such as total B-band luminosity and the average surface brightness and $(g-z)$ color

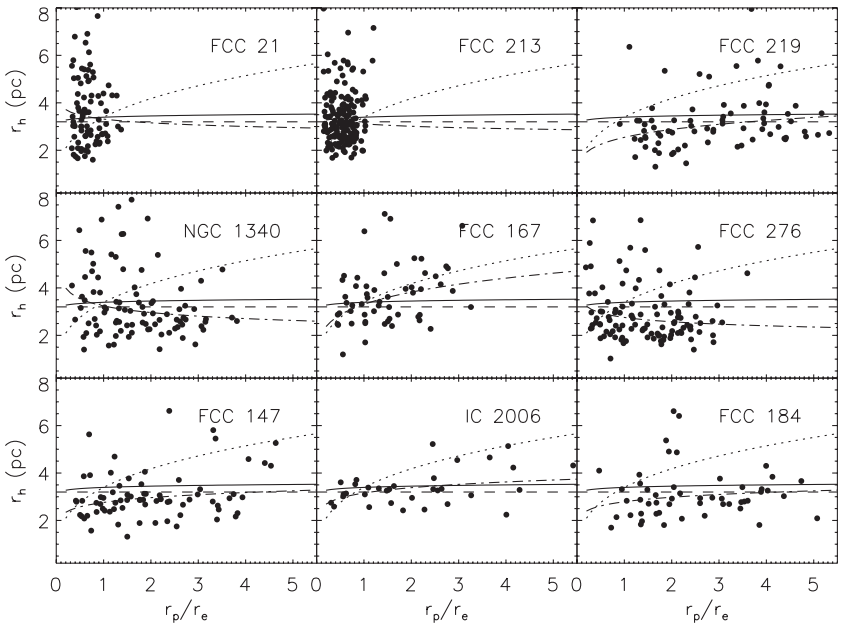

Figure 6. GC half-light radius (r_h) vs. galactocentric distance (in units of the galaxy effective radii) for blue GCs in the nine brightest galaxies in the Fornax cluster. The dot-dashed line shows the fits to the individual samples done in log–log space; the solid line is the weighted mean of the fits to the GC systems in all of the ACSFCS galaxies. These can be compared to a zero trend (dashed line: plotted at the mean r_h for all blue GCs of $r_h = 3.2$ pc), and the relation which would be seen in the MW GC system after projection effects are considered (dotted line).

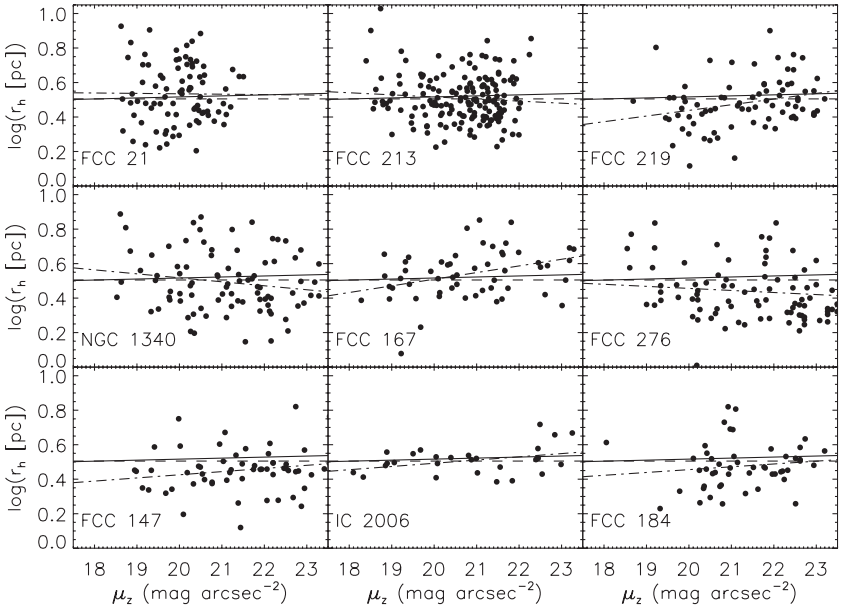

Figure 7. GC half-light radius [log(r_h)] vs. local galaxy surface brightness for blue GCs in the nine brightest galaxies in the Fornax cluster. The dot-dashed line shows the fits to the individual samples, the solid line is the weighted mean of all the fits to the GC systems in all of the ACSFCS galaxies. The dashed line shows a zero trend at the mean of the value of r_h for all blue GCs (3.2 pc).

within the effective radius. We use the half-light radius, r'_h corrected for local effects, and consider the blue ($(g-z)_{GC} < 1.05$) and red ($(g-z)_{GC} > 1.15$) GCs separately.

Figure 9 shows the result for blue GCs in our sample of early-type Fornax cluster galaxies. All blue GCs are shown; the solid circles show $\langle r'_h \rangle$ (biweight mean of r'_h) for each galaxy which has three or more blue GCs. We exclude FCC 21 (NGC 1316) from the fits as it is much more luminous than all other galaxies and has a peculiar GC size distribution (as shown in Section 3). The dotted line shows the trends with galaxy color and blue magnitude observed by J05. We find[11]

$$\log\langle r'_{h,\mathrm{blue,Fornax}}\rangle = 0.515(20) - 0.142(75)[(g-z)_{\mathrm{gal}} - 1.5],$$
$$\log\langle r'_{h,\mathrm{blue,Fornax}}\rangle = 0.500(18) + 0.023(07)(M_B + 20),$$
$$\log\langle r'_{h,\mathrm{blue,Fornax}}\rangle = 0.534(12) + 0.018(09)(\langle\mu_z\rangle - 19). \quad (2)$$

We refit the same relations to Virgo cluster galaxies—using a sample that is similar, but not identical, to that used in J05 (as discussed in Section 2)—and find:

$$\log\langle r'_{h,\mathrm{blue,Virgo}}\rangle = 0.453(10) - 0.225(45)[(g-z)_{\mathrm{gal}} - 1.5],$$
$$\log\langle r'_{h,\mathrm{blue,Virgo}}\rangle = 0.468(11) + 0.014(04)(M_B + 20). \quad (3)$$

Note that as well as this sample being slightly different to that used in J05 (possibly of particular importance here, some

[11] Note that we are using a short-hand notation for errors here, where $0.515(20) = 0.515 \pm 0.020$.

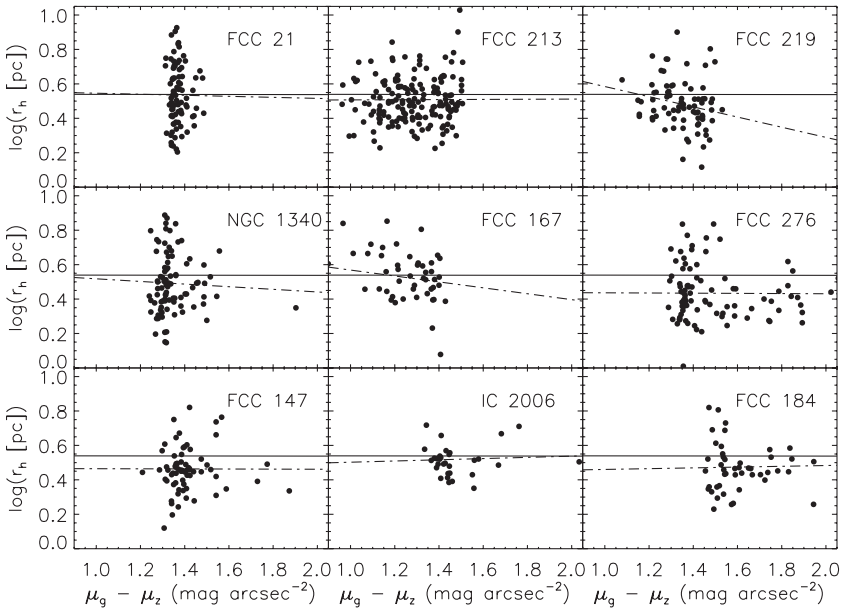

Figure 8. GC half-light radius [$\log(r_h)$] vs. local galaxy color ($\mu_g - \mu_z$) for blue GCs in the nine brightest galaxies in the Fornax cluster. The dot-dashed line shows the fits to the individual samples, the solid line is the weighted mean of all the fits to the GC systems in all of the ACSFCS galaxies. The dashed line shows a zero trend at the mean of the value of r_h for all blue GCs (3.2 pc).

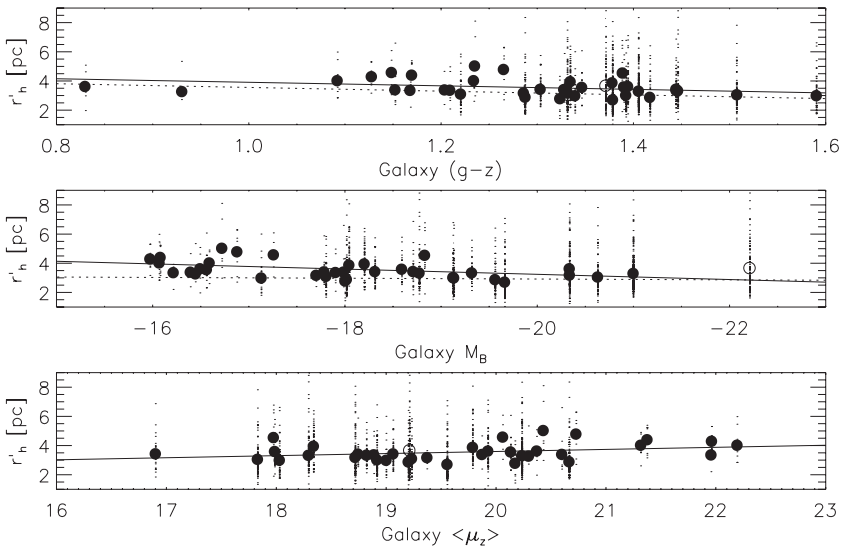

Figure 9. Top panel: r'_h vs. galaxy color for blue GCs. The filled circles show the biweight mean of the distribution for each galaxy which has three or more blue GCs. The solid line is fit to these averages. The open circle is the outlier FCC21 which is not included in the fits. Dotted lines show the fits from J05 to Virgo cluster galaxies. Middle panel: same, but for r'_h vs. galaxy total B-band magnitude. Bottom panel: same, but for r'_h vs. galaxy average surface brightness.

low-luminosity galaxies are added), the correction for local effects (a correlation of r_h with local surface brightness) is also slightly shallower than what was used in J05. These differences presumably explain the slight changes seen in the relationships we find and those reported by J05.

The slope of the $\log\langle r'_{h,\mathrm{blue}}\rangle$ versus galaxy color for Fornax galaxy GC systems is very slightly shallower than that observed for Virgo cluster galaxies (the same within 2σ); both are consistent with the -0.167 ± 0.054 found by J05. We find a trend with magnitude at the $\sim 3\sigma$ level in both the Fornax cluster and Virgo cluster galaxies (both the trend and the error on it are twice as large in Fornax than in Virgo), while the slope found for Virgo by J05 was consistent with zero within the 1σ errors. We attribute this difference to the slightly different samples and corrections for local effects as described above. J05 did not explore trends with the average surface brightness of the galaxy within the effective radius. In any case, we find this trend to be very small—only different from zero at about the 2σ level.

Repeating this analysis using red GCs in Fornax/Virgo cluster galaxies, we find slight differences such that the trends of size with color and magnitude for red GCs are slightly larger than for blue GCs. We still find that the trend with color is (slightly) larger in the Virgo cluster galaxies, while the trend with magnitude is larger in the Fornax cluster galaxies. The trend with average surface brightness is still consistent with zero (in fact, the sign flips). We also repeat the fits only including GCs within $5r_e$ in the Fornax cluster galaxies (and removing FCC 213 along which FCC 21 which was already not included) to make sure that these trends are not biased by the fact that the fainter, bluer galaxies typically have GCs to larger radial distances than the more massive ones. This cut does not significantly change the fits.

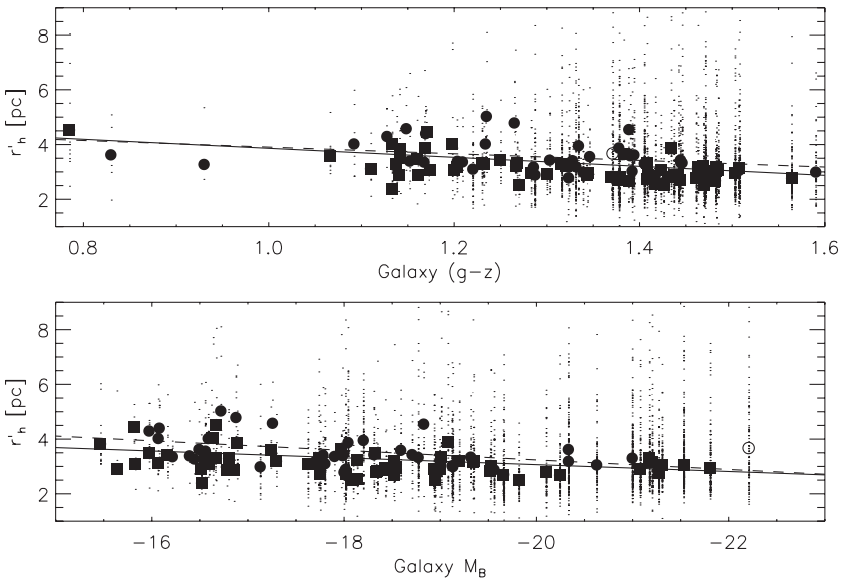

Figure 10. Same as Figure 9, but for blue GCs in both Fornax and Virgo cluster galaxies; biweight means for Fornax galaxies are shown as circles, for Virgo they are squares. The solid line are the fits to this data, dashed lines show the equivalent fits for just the blue GCs in Fornax galaxies (as in Figure 9).

These differences with the trends of half-light radius with global galaxy properties in Fornax early types versus Virgo early types and also with blue and red GCs suggests that care should be taken applying these corrections, and further study is needed to determine if there truly is a universal correlation. They may also point to interesting differences in the formation and evolution of GCs in Fornax cluster galaxies versus Virgo cluster galaxies and provide more constraints on the differences between the blue and red subpopulations of GCs. It is possible that different selection procedures for the dwarf galaxies included in the ACSVCS versus the ACSFCS could cause the differences between Virgo and Fornax. However, the impact of selection effects on the galaxies on trends of the average sizes of the GCs with global galaxy properties is likely to be complicated.

Figure 10 shows the same plot as in Figure 9, but for blue GCs in both Virgo and Fornax cluster galaxies combined. The fits in this case are

$$\begin{aligned}
\log\langle r'_{h,\mathrm{blue,both}}\rangle &= 0.473(10) - 0.209(41)[(g-z)_{\mathrm{gal}} - 1.5],\\
\log\langle r'_{h,\mathrm{red,both}}\rangle &= 0.409(10) - 0.575(91)[(g-z)_{\mathrm{gal}} - 1.5],\\
\log\langle r'_{h,\mathrm{blue,both}}\rangle &= 0.480(10) + 0.018(04)(M_B + 20),\\
\log\langle r'_{h,\mathrm{red,both}}\rangle &= 0.434(14) + 0.039(07)(M_B + 20). \qquad (4)
\end{aligned}$$

The addition of the systems in Virgo slightly reduces the significance of the trend with galaxy magnitude, and there is a clear difference in the average r'_h values between Virgo and Fornax for galaxies fainter than −18 mag (with Fornax GC systems having larger average r'_h than Virgo). The slope of the trend with galaxy color changes mostly because of the offset in zeropoint between Fornax and Virgo, combined with the distribution of colors of the galaxies in the two clusters (i.e., the slope for Virgo is parallel to but offset from that in Fornax).

Following J05, we argue that galaxy color and M_B should be almost equivalent as tracers of the global variation in r'_h. We show the color magnitude diagram for both ACSVCS and ACSFCS galaxies in Figure 11. In J05, it was shown that folding the linear variation of $\log r'_h$ with a quadratic relation describing the correlation between galaxy color and luminosity in the ACSVCS galaxies reproduces well the mild dependence

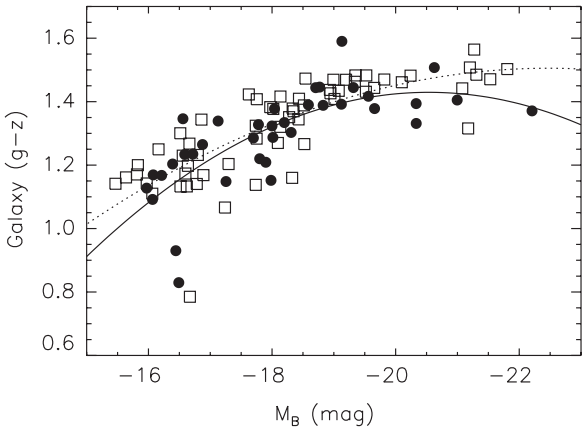

Figure 11. Color–magnitude diagram for all galaxies in the ACSVCS and ACSFCS. Fornax galaxies are shown as filled circles, while Virgo are open squares. The relation fit by J05 is shown as the dotted line. A quadratic fit to the Fornax data is shown by the solid line. The red outlier at $M_B \sim -19$ mag is FCC184, a face-on SB0 which may suffer from significant internal reddening.

of r'_h on M_B. We find indications of a steeper trend of average r'_h with galaxy magnitude in Fornax, and a shallower trend with galaxy color, even though there is no significant difference in the color–magnitude diagram. The biggest difference in the Virgo and Fornax color–magnitude diagrams shown in Figure 11 is that in the Fornax cluster the most luminous galaxies are not as red on average as they are in the Virgo cluster (Ferrarese et al. 2006, 2010). It is perhaps this slight blueward compression of the colors of Fornax early types which means that the color trend alone cannot explain all the dependence of GC size on galaxy mass. Among the Fornax cluster galaxies, the red outlier at $M_B \sim -19$ mag is FCC184, a face-on SB0 which may suffer from significant internal reddening. FCC 167 and FCC 26 (two galaxies with poor fits to the ACS images for which we use instead of the average color within r_e, the average color of regions used for the SBF measurement in Blakeslee et al. (2009)) are the bluest points at $M_B \sim -20$ and −16.5, respectively.

In order to fix the correlation of GC sizes with the mass of the galaxies, a trend with the galaxy magnitude and not just

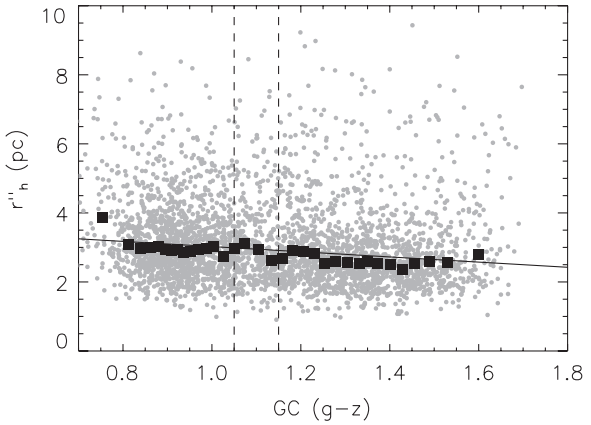

Figure 12. Corrected half-light radius, r_h'' vs. GC color for all GCs in all of our sample galaxies combined. The large squares show averages (biweight means) in bins of 0.15 mag of color. The solid line shows the best-fit linear relation of the form: $\log\langle r_h''\rangle \propto (g-z)_{\rm GC}$.

the color is needed, especially in low-luminosity Fornax cluster galaxies. However, the correlation between $\log r_h'$ and galaxy $(g-z)$ color that we find in both Fornax and Virgo cluster galaxy GC systems is consistent with J05, so we adopt the same correction to r_h'' used there,

$$r_h'' \equiv r_h' 10^{0.17[(g-z)_{\rm gal}-1.5]}, \quad (5)$$

or, combining with the correction for local environment (to r_h')

$$r_h'' \equiv r_h 10^{-0.008(\mu_z-21)+0.17[(g-z)_{\rm gal}-1.5]}. \quad (6)$$

We will return to the issue of a possible extra dependence of average r_h' value with magnitude in Section 6.

5.4. Dependence on GC Color

We now return to the issue of dependence of GC half-light radius on color, $(g-z)_{\rm GC}$. We use the half-light radius corrected for both local and global factors as described above, r_h''.

Figure 12 shows the corrected half-light radius, r_h'' versus GC color for all GCs in all of our sample galaxies combined. The large squares show averages (biweight means) in bins of 0.15 mag of color. The solid line shows the best fit to a linear relation of the form $\log\langle r_h''\rangle \propto (g-z)_{\rm GC}$, the best-fit slope is $b = -0.12 \pm 0.01$. This is similar to the relation found for GCs in Virgo galaxies by J05, who found $\log\langle r_h''\rangle \propto -(0.17\pm0.02)(g-z)_{\rm GC}$ but used a slightly different correction for local factors, as discussed above.

J05 contain a lengthy discussion of the correlation of GC color with galaxy color and luminosity. Less luminous, bluer ellipticals have GC systems which are usually metal poor, so have very few red GCs and therefore add little leverage to any trends of the GC sizes with GC color which will be dominated by the trends in more massive galaxies. In order to test that the correlation between half-light radius and GC color is the same in all colors and luminosities of galaxies, we follow J05 in defining subsamples of GCs in galaxies of similar colors. We exclude any galaxy which has extremely small numbers of very red GCs (they must have a number of GCs with colors $(g-z)_{\rm GC} > 1.3$ which is equal to at least 10% of the blue GCs $(g-z)_{\rm GC} < 1.05$), since these galaxies add little or no information about the color dependence of the half-light radius. We then create bins in galaxy color, by requiring at least 80 very red GCs ($(g-z)_{\rm GC} > 1.3$) in each bin; some bins have only a single galaxy.

The results of this exercise are shown in Figure 13. All subsamples are consistent with having $\log\langle r_h''\rangle \propto -(0.12\text{–}0.17)(g-z)_{\rm GC}$. Interestingly, there is quite a wide range of values of the extent of the galactocentric radii of the GCs (r_p/r_e) in these subsets, which vary from $r_p/r_e = 0.1$–1.2 (in the bin containing FCC 213) to $r_p/r_e = 0.5$–8.7 (in the bin containing FCC 63 and FCC 219). This argues against projection effects (Larsen & Brodie 2003) being the primary mechanism explaining the r_h–color correlations. Beyond the large ACSVCS and ACSFCS samples, other studies of the dependence of r_h with GC color also suggest that this dependence is at least partly intrinsic to the clusters (see Section 3.2 of Harris et al. 2009b for a summary of this evidence; note that an earlier claim by Spitler et al. 2006 that projection effects are responsible for the r_h–color correlation in the Sombrero galaxy has been revised in Harris et al. 2009b). Possible mechanisms for creating this intrinsic dependence of size and color have been given in Jordán (2004) and Harris (2009).

6. FINAL CORRELATIONS OF HALF-LIGHT RADIUS

In this section, we list the final correlations of the half-light radius of the GCs in Fornax cluster galaxies with internal, local, and global environmental variables (as listed in Section 4). We find subtly different scaling relations for the size of GCs in Fornax cluster galaxies than were found by J05 in Virgo cluster galaxies. We find that the trend with local environment (measured by local surface brightness) may be a bit flatter in the Fornax cluster galaxies than in Virgo cluster galaxies ($b_{\mu,\rm Fornax} = 0.006 \pm 0.003$ as opposed to $b_{\mu,\rm Virgo} = 0.011 \pm 0.003$, while the combined sample gives $b_\mu = 0.008 \pm 0.002$). After applying this local correction, we look at correlations with global properties of the galaxies and find a similar trend of average size with galaxy color as was found in the GC systems of Virgo cluster galaxies, but there is some evidence that an extra correlation with galaxy magnitude might be present in the GC systems of Fornax dwarfs. After applying both corrections for local and global properties finally, we find a slightly shallower trend of GC size with GC color ($\log\langle r_h''\rangle \propto -0.12(g-z)_{\rm GC}$ versus $\log\langle r_h''\rangle \propto -0.17(g-z)_{\rm GC}$ in Virgo cluster galaxy GCs).

We therefore use corrected radii

$$\hat{r}_h \equiv r_h 10^{-0.008(\mu_z-21)+0.17[(g-z)_{\rm gal}-1.5]+0.12[(g-z)_{\rm GC}-1.2]}. \quad (7)$$

We also consider an extra correction of

$$\hat{r}_h' \equiv \hat{r}_h 10^{-0.02[M_B+21]}, \quad (8)$$

which is only important for galaxies with $M_B \gtrsim -19$ mag in the Fornax cluster.

These subtle differences in the trends raise clear questions about the applicability of using the average half-light radii of GCs belonging to low-luminosity galaxies as a distance indicator. On the other hand, this may be hinting at an interesting difference between the formation/evolution of GC systems in dwarf galaxies in the Virgo cluster versus the Fornax cluster—possibly as a result of the different environments.

We provide in Table 3 a listing of the ACSFCS galaxies for which we have r_h measurements. Galaxies are ordered by absolute B-band magnitude. Also included in this table are the measured color of the galaxy, average surface brightness at the position of the GCs, average color of the GCs, and the

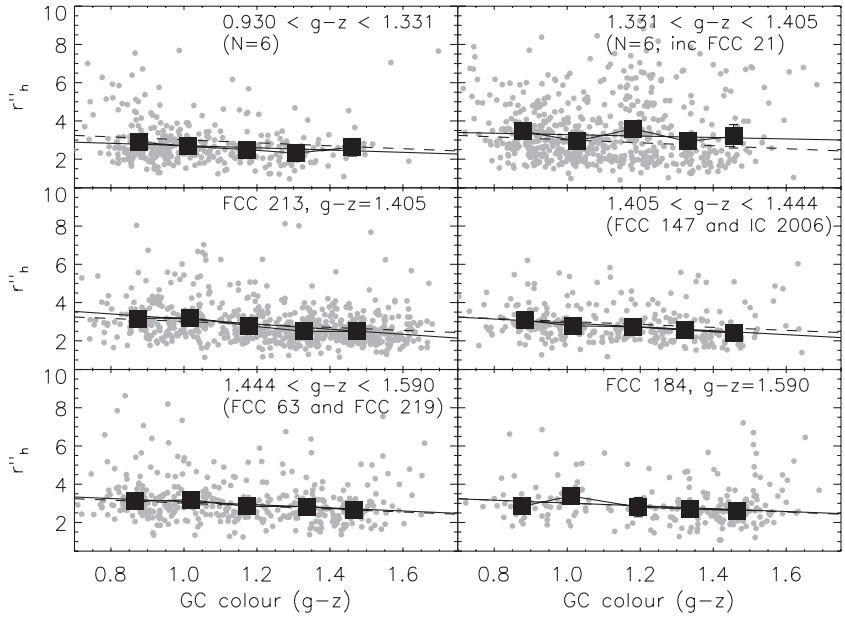

Figure 13. Same as Figure 12, but in subsamples separated by galaxy color (as indicated). The dashed line in each panel shows the fit to the entire sample in Figure 12.

Table 3
Summary of GC Sizes in Fornax Cluster Galaxies

Galaxy	M_B	$(g-z)_{\rm Gal}$	$\langle\mu_z(r_p)\rangle$	$N_{\rm GC}$	$\langle(g-z)_{\rm GC}\rangle$	$\langle r_h\rangle('')$	$\langle\hat{r}_h\rangle('')$	$\langle\hat{r}'_h\rangle('')$
FCC 21	−22.21	1.37	20.07	1.12	232	0.040(02)	0.038(02)	0.040(02)
FCC 213	−21.00	1.41	20.63	1.26	698	0.028(01)	0.027(01)	0.027(01)
FCC 219	−20.63	1.51	21.08	1.19	220	0.029(01)	0.029(01)	0.029(01)
NGC 1340	−20.33	1.33	21.14	1.00	137	0.030(02)	0.027(02)	0.026(02)
FCC 167	−20.33	1.09	20.69	1.24	266	0.032(01)	0.031(01)	0.030(01)
FCC 276	−19.66	1.38	21.51	1.11	232	0.025(01)	0.023(01)	0.022(01)
FCC 147	−19.56	1.42	21.76	1.15	201	0.028(01)	0.026(01)	0.025(01)
IC 2006	−19.32	1.44	21.31	1.15	89	0.034(02)	0.033(02)	0.030(02)
FCC 184	−19.13	1.59	21.44	1.29	216	0.030(01)	0.031(01)	0.028(01)
FCC 83	−19.12	1.39	21.55	1.08	173	0.032(01)	0.029(01)	0.027(01)
FCC 193	−18.83	1.39	21.09	1.08	23	0.046(06)	0.043(06)	0.039(05)
FCC 63	−18.77	1.45	21.91	1.07	142	0.034(02)	0.032(02)	0.029(01)
FCC 170	−18.71	1.44	21.89	0.98	30	0.030(04)	0.027(03)	0.025(03)
FCC 153	−18.59	1.39	21.34	0.92	28	0.037(04)	0.033(04)	0.029(03)
FCC 177	−18.31	1.30	22.82	0.96	47	0.038(03)	0.032(02)	0.028(02)
FCC 249	−18.20	1.33	22.65	1.00	102	0.036(02)	0.031(02)	0.027(02)
FCC 190	−18.04	1.38	22.08	0.98	103	0.041(02)	0.036(02)	0.032(02)
FCC 47	−18.01	1.29	22.62	1.05	184	0.032(01)	0.027(01)	0.024(01)
FCC 310	−18.00	1.32	20.64	0.93	18	0.028(04)	0.024(04)	0.021(03)
FCC 43	−17.98	1.15	20.81	1.03	15	0.036(06)	0.030(05)	0.026(04)
FCC 148	−17.90	1.21	21.41	1.02	13	0.035(07)	0.030(05)	0.026(05)
FCC 255	−17.80	1.22	22.56	0.99	57	0.035(03)	0.029(03)	0.025(02)
FCC 277	−17.78	1.33	21.61	1.01	17	0.034(03)	0.030(03)	0.026(03)
FCC 55	−17.70	1.29	20.49	1.08	12	0.034(04)	0.030(04)	0.026(03)
FCC 152	−17.25	1.15	21.04	0.86	5	0.050(21)	0.040(16)	0.034(14)
FCC 143	−17.13	1.34	22.83	0.94	33	0.033(04)	0.028(03)	0.023(03)
FCC 95	−16.88	1.26	24.51	0.99	13	0.049(11)	0.040(09)	0.033(07)
FCC 204	−16.72	1.23	22.08	0.85	7	0.050(20)	0.040(16)	0.033(13)
FCC 136	−16.59	1.23	22.62	0.97	13	0.045(05)	0.038(04)	0.031(03)
FCC 182	−16.56	1.35	23.29	1.02	22	0.039(05)	0.034(04)	0.028(03)
FCC 26	−16.49	0.64	22.03	1.01	14	0.041(08)	0.029(06)	0.024(05)
FCC 90	−16.44	0.93	21.71	0.99	8	0.040(10)	0.030(08)	0.024(06)
FCC 106	−16.39	1.20	21.43	1.07	5	0.042(20)	0.036(17)	0.029(14)
FCC 324	−16.21	1.17	22.80	0.89	7	0.036(07)	0.028(05)	0.022(04)
FCC 203	−16.08	1.17	22.76	0.91	10	0.046(07)	0.036(06)	0.029(05)
FCC 100	−16.07	1.09	23.10	0.94	9	0.044(12)	0.034(09)	0.027(07)
FCC 303	−15.97	1.13	22.89	0.95	10	0.051(09)	0.040(08)	0.031(06)

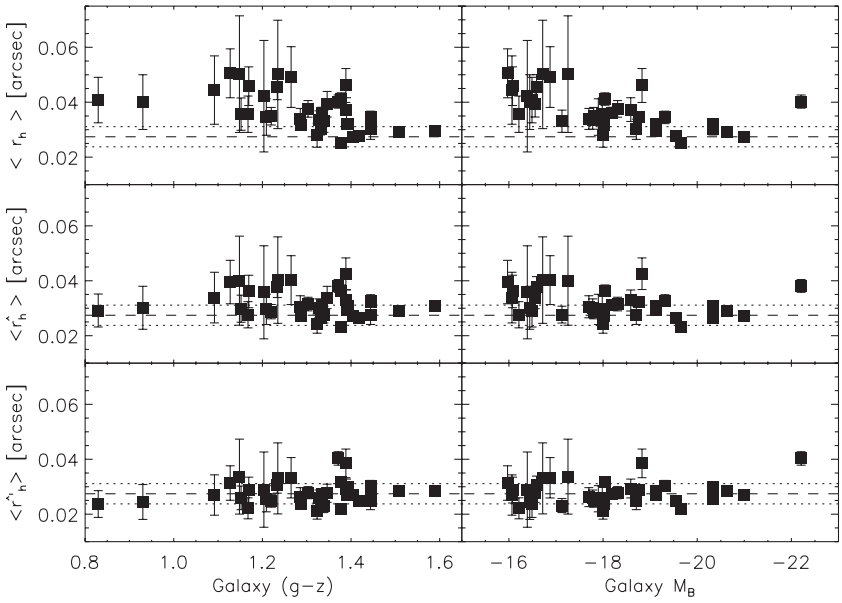

Figure 14. Corrected, $\hat{r}_h$ (middle panel; corrections for galaxy and GC color and local disk surface brightness), extra corrected (lower panel: including a galaxy magnitude term) and uncorrected, r_h (top panel) vs. galaxy color and magnitude for all galaxies in the sample. The dashed lines show the biweight mean of the extra corrected values excluding FCC 21 (dotted lines show the sigma, also calculated using a biweight location estimator). Error bars on the points are the 95% confidence internals on the means for each galaxy.

average sizes of the GCs (raw, corrected, and "extra corrected"). Figure 14 shows the corrected $\langle \hat{r}_h \rangle$, extra corrected $\langle \hat{r'}_h \rangle$, and uncorrected, $\langle r_h \rangle$ versus galaxy color and magnitude for all galaxies in the Fornax sample. The dashed lines show the biweight mean of the extra corrected values excluding FCC 21 (dotted lines show the sigma, also calculated using a biweight location estimator). Error bars on the points are the 95% confidence intervals on the means for each galaxy. It is clear that after the corrections are applied the value of $\langle \hat{r}_h \rangle$ is remarkably consistent over galaxy color and magnitude. Nevertheless, two outliers are obvious, having larger than usual values of $\langle \hat{r}_h \rangle$. The first (at $M_B \sim -22$) is FCC 21 (NGC 1316 or Fornax A), which was noted earlier as a merger remnant showing a peculiar distribution of GC half-light radii. The second (at $M_B \sim -19$) is FCC193, an S0 galaxy close to the center of the Fornax cluster. Unlike J05, we do not find that the average r_h is consistent with being constant after just corrections for galaxy and GC color and local surface brightness of the disk. We find that, in Fornax dwarfs, the average value of r_h is larger than expected (as is apparent from the middle panel of Figure 14).

7. DISCUSSION

7.1. Half-light Radius as a Distance Indicator

Despite the differences in the environmental trends of GC half-light radius examined here, we begin this section by re-emphasizing how little the average sizes of GCs actually vary from galaxy to galaxy. The observed trends are all very mild and result in only small changes in the average half-light radii over significant changes in host galaxy color and luminosity. This is particularly true in the case of the brightest early-type galaxies in which the uncorrected mean half-light radius of the GC system already offers a distance indicator with errors comparable to those from the best techniques currently available (i.e., $\sim$ 10%–15%).

We now consider in more detail the use of mean half-light radius as a distance indicator. We first examine only the bright early-type galaxies ($M_B < -19$ mag) in which we have shown that the uncorrected mean half-light radius is very close to constant. Figure 15 shows both uncorrected and corrected average r_h values for bright galaxies ($M_B < -19$ mag) in Fornax and Virgo, and also NGC 4697 and VCC 575. The values follow very closely the expected scaling for a constant mean half-light radius. The line is not a fit to the data, but simply this relation normalized to a value of $\langle r_h \rangle = 0\farcs033$ (solid line) at $D = 16.5$ Mpc which is the average value found for Virgo giants (both in this work and in J05).

A simple comparison of the biweight average of all the average values of uncorrected r_h in GC systems of bright Fornax and Virgo early-type galaxies implies a Fornax distance of 18.6 $\pm$ 1.0 Mpc (based on a Virgo distance of 16.5 Mpc; Mei et al 2007). Note that the error estimate includes only the dispersion in the values of $\langle r_h \rangle$ in both Fornax and Virgo systems; the systematic error on this from the measurement of the GC sizes is 2.8 Mpc. The significant outlier in the Fornax galaxies is FCC 21 which, as we discussed before, has a peculiar distribution of r_h values.[12] Excluding FCC21 from the averaging for Fornax, we find 19.1$\pm$0.9 $\pm$ 2.5 Mpc. The dispersion in the uncorrected value of $\langle r_h \rangle$ is $0\farcs0041$ (13%) for all systems in Fornax cluster bright early types, but FCC 21 accounts for almost half of this value—by excluding FCC21 it drops to $0\farcs0031$ (11%).

Applying the corrections discussed in Sections 6 and 7 above (note we apply our corrections to the GC systems in both Fornax and Virgo), we find a mean angular size of $0\farcs0293$, with dispersion $0\farcs0041$ for all bright Fornax early types ($0\farcs0285$ and $0\farcs0031$ excluding FCC 21), while for Virgo we find $0\farcs0331$ and $0\farcs0032$. This then implies a Fornax distance of $D = 18.6 \pm 0.9 \pm 2.5$ Mpc (19.1$\pm$0.8 $\pm$ 2.7 Mpc excluding FCC 21), if the distance to Virgo is 16.5 Mpc. The dispersion in the value of the corrected mean half-light radius in Fornax

[12] We note that FCC 21 would be readily identified as a peculiar early-type galaxy in any data set where the r_h of GCs can be measured, as the prominent dust lanes would be clearly seen. An r_h-derived distance on such a galaxy could be potentially affected by a large systematic error.

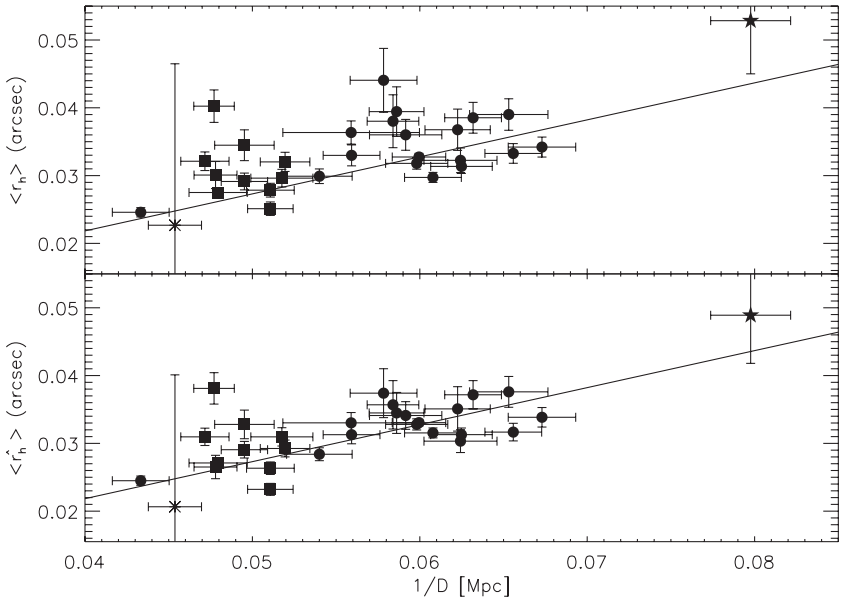

Figure 15. Top panel: Average values of r_h (no corrections) vs. inverse distance for the giant galaxies ($M_B < -19$ mag) in Fornax (squares) and Virgo (circles). Also includes NGC 4697 (star) and VCC 575 (asterisk). The lower panel shows the same, but for average r_h values corrected for dependencies on GC and galaxy color, and local disk surface brightness. The solid line shows the calibration of $r_h \propto 1/D$ from J05 (normalized to 0.″033 at $D = 16.5$ Mpc, which is also the average value we find for Virgo giant galaxies).

early types is 14% (11% excluding FCC 21) comparable to the dispersion found by J05 for Virgo cluster systems.

The above discussion relies on an assumed mean distance to Virgo to test the reliability of the method. We can also use the SBF distances to the galaxies in both Virgo and Fornax to provide an updated calibration of the method. Using a biweight mean of all the corrected mean half-light radii of giant galaxies in both the Fornax and Virgo clusters (but excluding FCC 21), we find a distance in Mpc of

$$D = \frac{0.561 \pm 0.010 \pm 0.060}{\langle \hat{r}_h \rangle} \text{ Mpc}, \quad (9)$$

where $\langle \hat{r}_h \rangle$ is in arcseconds. This is based on a constant value of $\langle \hat{r}_h \rangle = 2.71 \pm 0.05 \pm 0.25$ pc for a GC with color $(g-z) = 1.2$, in a galaxy with color $(g-z)_{\rm gal} = 1.5$ and at an underlying surface brightness of $\mu_z = 21$ mag arcsec^{-2} [note that one prefers to use *uncorrected* r_h values in giant galaxies in both Virgo and Fornax, the result is $\langle r_h \rangle = 2.84 \pm 0.07 \pm 2.9$ pc, so the calibration is then $D = (0.585 \pm 0.010 \pm 0.060)/\langle r_h \rangle$ Mpc].

Finally, we can also use the geometric calibration based on the sizes of GCs in the MW of $\langle \hat{r}_h \rangle \simeq 2.54 \pm 0.1$ pc calculated by J05 to provide a distance to the Fornax cluster independent of other extragalactic distance ladder steps. Using our mean corrected $\langle \hat{r}_h \rangle$ for Virgo and Fornax, respectively, we find distances of $15.8 \pm 0.7 \pm 1.4$ Mpc and $17.9 \pm 1.1 \pm 1.8$ Mpc ($18.4 \pm 1.0 \pm 1.9$ Mpc excluding FCC21). These distances are reassuringly close to measurements using other techniques (see, e.g., the discussion in Blakeslee et al. 2009). Note that the quoted errors are statistical, plus the systematic error on measuring the half-light radii on ACS images. Systematic errors introduced by comparing the size of GCs in early types to those in the MW can be estimated at about 15%–20%. We estimate that the best distance to Fornax from this method is 18.4 ± 3.7 Mpc (where FCC21 has been excluded).

We also show in Figure 16 the same plot for *all* galaxies in Virgo and Fornax together (i.e., also including the fainter galaxies with smaller numbers of GCs) to illustrate the impact of the environmental corrections on how the GC systems in the fainter galaxies fall on the relation. If we use all galaxies together, we estimate a distance to Fornax of $D = 17.2 \pm 0.6 \pm 1.9$ Mpc if no corrections are applied, $D = 17.6 \pm 0.4 \pm 2.3$ Mpc if the general corrections (for GC color, local surface brightness at the position of the GC, and host galaxy color) are applied, and $D = 20.2 \pm 0.6 \pm 2.8$ Mpc if the extra correction on host galaxy luminosity is applied to the sizes of the Fornax cluster galaxy GCs. We note that this final measurement is very close to the 20.0 ± 1.4 Mpc recently found by Blakeslee et al. (2009) using the SBF method.

Our prescriptions to correct r_h for it to be useful as a standard ruler depend on the particular observational setup of our program in that the corrections are given using magnitudes measured in g and z. This limits their usefulness for other observational setups to some extent, but does not preclude their use. First, as we have shown above, the *uncorrected* mean half-light radius is a good distance indicator for bright galaxies ($M_B < -19$).[13] These are the class of galaxies where obtaining a distance using r_h would be most useful, as they provide large numbers of GCs that are necessary to reduce the statistical uncertainty in $\langle r_h \rangle$. In case of a lower luminosity galaxy observed in other bands, population synthesis models for early-type galaxies and GCs can be used to transform from our bands to the bandpasses under consideration. Alternatively, galaxies in well-observed galaxy clusters such as Virgo, or MW GCs, could be used to infer empirical transformations to the chosen bandpasses if the appropriate data exist. This is a more involved procedure, but as pointed out above, measuring distances using $\langle r_h \rangle$ is not ideally suited for low-luminosity galaxies in any case, due to the small number of GCs generally available in such galaxies. Finally, we note that our calibration for $\langle r_h \rangle$ hinges on the use of a King model to derive the

[13] It can be argued that a distance needs to be known first in order to know if measuring a distance with uncorrected r_h is appropriate. But there are other ways the nature of a galaxy as a luminous elliptical could be established at the required level of precision: e.g., by its relative luminosity to other galaxies in the case of a cluster of galaxies.

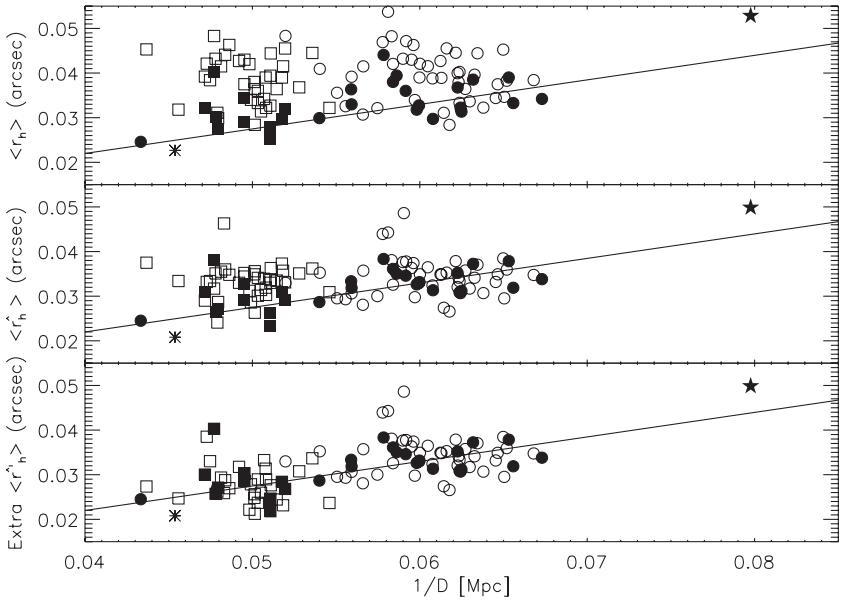

Figure 16. Same as Figure 15, but now showing both giant and dwarf galaxies, and also including the extra magnitude correction for Fornax dwarfs (this is only applied to the GC sizes in Fornax, not in Virgo, NGC 4697, or VCC 575). Dwarfs are shown as open symbols, giants as filled. Fornax cluster galaxies are squares, Virgo are circles, NGC 4697 is the star, and VCC 575 is the asterisk. We omit error bars for clarity—the size of the errors can be seen in Figure 15.

size of GCs, and presumably the use of other models could lead to some systematic differences in the measured half-light radii. Fortunately, it is possible to calibrate away these potential differences by using the publicly available data of the ACSVCS galaxies. All our measured r_h for GCs belonging to those galaxies have been published in Jordán et al. (2009). If using a different model translates into a systematic difference with the r_h measurements presented in Jordán et al. (2009), this difference can be then be taken into account.

7.2. Half-light Radii as Tracers of GC Formation and Evolution

It is remarkable how little the mean half-light radius of GC systems varies in early-type galaxies in both the Fornax cluster and the Virgo cluster. The variation is only about 20% over half a magnitude change in galaxy color and 3 orders of magnitude in galaxy luminosity; when only luminous ($M_B < -19$ mag) galaxies are considered, the variation is still smaller. This property clearly provides a significant constraint on models of GC formation and evolution. A successful model must also account for the red GCs being ∼20% smaller than blue ones, for the lack of dependence of GC size on luminosity (or mass), and for the differing trends of GC half-light radius with galactocentric distance hinted at in early types (where the trend is mild) and late types (where it is much steeper).

In J05, two simple models for the formation of GCs were pitted against some of the observational trends of the half-light radii. The first was a model in which the half-light radius of the GCs is determined by overall pressure confinement of the proto-GC cloud (e.g., McLaughlin & Pudritz 1996), while a second model was considered in which the radius is a consequence of tidal limitation of the GCs. Both models immediately run into a problem of predicting a scaling of half-light radius with GC mass (or luminosity) which is significantly larger than the almost zero trend that is observed ($r_h \sim M^{1/2}$ and $r_h \sim M^{1/3}$, respectively). Thus, in both cases an unknown mechanism is required—possibly related to a scaling of star formation efficiency with cloud binding energy. Assuming such a mechanism exists, J05 went on to show that in the pressure-confined case there is only a mild dependence of the mean half-light radius with galaxy luminosity ($\langle r_h \rangle \propto L^{-0.12}$), while in the tidal limitation model the dependence is exactly zero (i.e., $\langle r_h \rangle \sim L^0_{\rm gal}$). They therefore argued that both models could predict the negligible trend of mean half-light radius with galaxy luminosity observed in ACSVCS galaxies.

In this paper, we observe a slight dependence of $\langle r'_h \rangle$ on galaxy luminosity in both Fornax and Virgo cluster early-types which clearly differs from the almost zero trend observed in the GC systems of Virgo cluster early types by J05 (note that slight differences in the Virgo cluster GC sample, and treatment of local factors may account for this difference). We observe that for blue GCs the scaling of size with luminosity is $\langle r'_h \rangle \propto L^{-0.05\pm0.02}$ and for red GCs it is $\langle r'_h \rangle \propto L^{-0.11\pm0.04}$. A possible explanation of the difference between the subpopulations could be that as the red GCs tend to be concentrated more toward the center of the galaxy they may be more significantly impacted by the size of the galaxy (i.e., the depth of its potential well). Overall, this evidence of a mild galaxy luminosity dependence of GC sizes, slightly favors the pressure confinement scenario over the tidal limitation model, especially for the red subpopulation, however since the trends are so marginal, and appear to depend on the GC selection procedure, we do not consider this strong evidence.

We also see some small evidence for a shallower trend of the GC sizes with local surface density of the host galaxy in the Fornax galaxies than was observed in the Virgo galaxies as well as a slightly shallower trend with GC color (once global and local correlations are corrected for). Such subtle differences in the environmental dependencies of the sizes of the GCs in Fornax cluster galaxies versus Virgo cluster galaxies may be hinting at a dependence of the formation mechanisms or more likely the structural and dynamical evolution of GCs on the global environment of the host galaxies.

As in J05, the slope of the relation between half-light radius and galactocentric distance (b_r) is significantly lower than is found for GCs in the MW, which (after projection effects are considered) follow a relation with $b_{r,\rm MW} \sim 0.3 \pm 0.15$.

This study then further confirms the discrepancy between the galactocentric trends in early types and in the MW; however, we note that our selection removes GCs with $r_h > 10$pc (as discussed in Jordán et al. 2009) which could be driving the large trend seen in the MW GC system. If real, this difference in the GC systems is clearly of interest for further study and may point to a difference in the formation or dynamical evolutions of GCs in early-type galaxies versus late-type galaxies or, possibly, of galaxies in low-density environments versus clusters.

There have been other recent papers which take advantage of the ACS on *HST* to measure the half-light radii of GCs in galaxies outside the LG and study their behavior with galactocentric distance. DeGraaff et al. (2007) show that the GCs in NGC 1533 (an SB0 galaxy in the Dorado group which appears to be transitioning from late to early type) have a r_h versus galactocentric radius relation more similar to the GCs in the MW than in Virgo or Fornax cluster early-type galaxies. Spitler et al. (2006) study the GC system of the Sombrero galaxy, an Sa or S0 galaxy also in the transition region between late and early types and see similar behavior (they find $b_{\rm blue} = 0.16 \pm 0.04$, $b_{\rm red} = 0.32 \pm 0.05$, and $b_{\rm all} = 0.24 \pm 0.03$ using the same notation we use above). Harris et al. (2009a) studied GC candidates in NGC 891 (a nearby edge-on spiral thought to be similar to the MW) and while the numbers of GCs in NGC 891 are quite small the noisy trend seen with galactocentric radius seems consistent with that seen in the MW. These studies are indicative of a general property of the GC systems in late-type galaxies in small groups to have a steeper dependence on galactocentric radius than is seen in the systems of early-type galaxies in clusters; however, the statistics here are still very small. It would be interesting to study the GC systems of more late-type galaxies to test this hypothesis. At the moment, it cannot be determined if it is the galaxy morphology or the environment in which the galaxy resides that drives this change. A study of GC systems of early types in low-density environments and late types in higher density environments would be instructive to disentangle the effects of morphology and density. DeGraaff et al. (2007) tentatively explain the difference as the effect of steeper density gradients in small groups like Dorado or the LG versus large clusters. Since the sizes of GCs may be limited by tidal fields, the argument is that GC sizes should have a stronger dependence on radius in small groups than in clusters. We find here a (marginally) smaller trend of GC radius on galactocentric radius for the GC systems in Fornax cluster galaxies than in the Virgo cluster and while Virgo is the larger cluster, the central density of Fornax is about twice that of Virgo in term of galaxies per Mpc^3 (see Table 1 of Jordán et al. 2007a). Based on this measure of density, we may then be observing the trend expected by the DeGraaff et al. (2007) model.

It is also interesting that while the size–galactocentric radius relation appears to point to differences in the GC systems of different Hubble types (or galaxies in difference environments), recent studies of the dispersion of the GCLF instead favor the idea that GC systems in late-type galaxies (specifically the MW and the M31) are not different from those in early types since they fit on the same dispersion–luminosity relation of systems in early types (Jordán et al. 2007b). The color distribution of the GC systems of late and early types have also been shown to be similar and have similar trends with galaxy luminosity (Peng et al. 2006). At the moment, the only evidence suggesting a significant difference between the GC systems in late and early-type galaxies is the change in the size–galactocentric radius relation. Clearly, further work, including studies to significantly greater galactocentric radii, need to be done to confirm this as a general property.

8. CONCLUSIONS

We have used data on the half-light radii of GCs belonging to galaxies observed in the ACSFCS to extend the work of J05 in which the environmental dependencies of the half-light radii of GCs in early-type galaxies in the ACSVCS were studied, and a corrected mean half-light radius was suggested as a reliable distance indicator. By adding data from the ACSFCS, we increase the sample size for the study of the environmental dependencies, and add leverage to the study of the corrected half-light radius as a possible distance indicator (since Fornax is at a larger distance than the Virgo cluster).

We find only subtle differences in the environmental dependencies of the sizes of GCs in Fornax cluster galaxies from what was found in the Virgo cluster by J05. In addition, we perform a PCA to check that no major correlations are being hidden (in the Appendix).

Looking at 2D relations, we again confirm the well-known results that there is no correlation between GC size, r_h, and mass (for $M < 2 \times 10^6\ M_\odot$, but that blue GCs ($(g-z) < 1.05$ with $\langle r_h \rangle = 3.36 \pm 0.03 \pm 0.25$ pc) are about 20% larger than red ones ($(g-z) > 1.15$ with $\langle r_h \rangle = 2.83 \pm 0.02 \pm 0.25$ pc).

We show that the half-light radii of GCs in early-type galaxies in the Fornax cluster increase only slightly with galactocentric radius (or decreasing surface brightness), as was also found by J05 for systems in Virgo cluster early types. In fact, the trend we find in Fornax cluster systems is slightly shallower than that seen in the Virgo cluster. As was found in J05, the trend of r_h with galactocentric distance is significantly shallower (only 2σ different from zero in Fornax galaxy GC systems) than that observed in our Galaxy perhaps pointing to a different formation scenario, or evolution of GCs in early types versus late types (or in high-density regions versus low-density regions). We discuss this observation in light of other recent studies of the GC systems of late-type galaxies and argue that there is now some evidence for a general property of the GC systems of late-type galaxies in small groups to have a stronger trend of half-light radius with galactocentric distance than is seen in early types in clusters. This will provide stronger constraints on the differences in formation and evolution of GCs in different types of galaxies in different environments.

We confirm the trend of mean half-light radius with galaxy color that was first observed in J05, but show suggestions that there is a residual correlation with galaxy luminosity in the mean half-light radius of GC systems of Fornax early-type galaxies which is larger than that seen in GC systems of Virgo early types. We revisit the two simple pictures of the origin of r_h in GCs discussed by J05, arguing that the additional trend we observe for the mean half-light radius of GC systems in both Fornax and Virgo cluster early-type galaxies to decrease with galaxy luminosity (as $\langle r_h' \rangle \propto L^{-0.05\pm0.02}$ in blue GCs and $\langle r_h' \rangle \propto L^{-0.11\pm0.04}$ in red GCs) may be providing some support for the "pressure-confined proto-GC cloud" model over tidal limitation of r_h. However, since the size of this trend appears to depend on the details of the GC selection (as it was not present in the similar J05 sample), we suggest that it should not be over interpreted.

We show that for the most luminous galaxies ($M_B < -19$ mag), the uncorrected mean half-light radius is by itself an

excellent distance indicator, varying by around 10%–15% across galaxies. This is especially true if we remove the unusual GC system of FCC 21 (Fornax A). Once corrected for dependencies on GC and galaxy color and local surface brightness, we find a constant value of $\langle \hat{r}_h \rangle = 2.71 \pm 0.05 \pm 0.25$ pc for a GC with color $(g-z) = 1.2$, in a galaxy with color $(g-z)_{\rm gal} = 1.5$ and at an underlying surface brightness of $\mu_z = 21$ mag arcsec^{-2} across giant galaxies in both the Virgo and Fornax clusters (for Virgo alone, we find $\langle \hat{r}_h \rangle = 2.67 \pm 0.07 \pm 0.25$ pc, in Fornax it is $\langle \hat{r}_h \rangle = 2.78 \pm 0.12 \pm 0.25$ pc excluding FCC21). The same simple geometric calibration used by J05 to estimate an independent distance to the Virgo cluster of $D_{\rm Virgo} = 16 \pm 2.3$ Mpc gives a distance to the Fornax cluster of $D_{\rm Fornax} = 18.4 \pm 3.7$ Mpc (excluding GCs in FCC 21).

This extension of the work of J05 to include GC systems in early-type galaxies in the Fornax cluster adds support to the idea of a constant mean r_h in luminous early-type galaxies, but suggests that the environmental dependencies may be subtly different in different environments which is especially important in the lower mass galaxies. The mean half-light radii in GC systems of massive early-type galaxies has the potential to provide a geometric distance measurement to bright early-type galaxies, which could reach cosmologically interesting distances (as quantified by J05) in the era of giant optical telescopes with adaptive optics.

Support for programs GO-10217 and GO-9401 was provided through grants from the Space Telescope Science Institute, which is operated by the Association of Universities for Research in Astronomy, Inc., under NASA contract NAS5-26555. K.L.M. acknowledges funding from the Peter and Patricia Gruber Foundation as the 2008 Peter and Patricia Gruber Foundation International Astronomical Union Fellow, and from the University of Portsmouth. A.J. and L.I. acknowledge support from the Chilean Center of Excellence in Astrophysics and Associated Technologies PFB-06, and from the Chilean Center for Astrophysics FONDAP 15010003. A.J. acknowledges additional support from MIDEPLAN ICM Nucleus P07-021F.

APPENDIX

PRINCIPAL COMPONENT ANALYSIS

PCA provides a statistical method to search for correlations between two or more correlated variables. Since (as described in Section 4) the size of a GC may depend on several interrelated properties of the host galaxy, local galaxy environment and of the GC itself, the problem is an ideal candidate for a PCA. PCA decomposes the observed correlations between parameters into a set of eigenvectors and eigenvalues describing the main variance seen in the data. This method is now becoming a standard in astronomical applications where intercorrelations between several variables are common, so we do not provide a full explanation of the method here, but rather refer the reader to standard references below. Here we use the PCA routine in the Astronomy IDL Library[14] (which performs PCA according to the method described in "Multivariate Data Analysis" by Murtagh & Heck 1987). We follow closely the method described in Woo et al. (2008) in the interpretation of the PCA results and in the use of bootstrap re-sampling to calculate the errors.

The goals of our PCA will not be to derive expressions for the dependence on r_h on other factors, but rather to look at the shape of the trends we expect to see and which relations we expect to be important and unimportant. In a sense, we use this to arrive at the optimal number of parameters to describe the r_h variations. Traditional 2D relations are easier to interpret so we will return to them in the main body of the paper (Section 5) once we understand the overall shape of the expected interdependencies.

We initially perform a PCA on Fornax cluster GCs using all eight environmental factors described in Section 4 (in log, or magnitude space) as well as $\log r_h$. Numerical results are shown in Table 4. In this table (and Tables 5, 6, and 7 below), the eigenvector outputs (describing the directions of the main variance in the data) are labeled at Vi (for a PCA with n variables, $i = 1...n$). We list the projection of each input variable onto these eigenvectors as well as the eigenvalue ("E-value") expressed as a percentage of the total. We also show the ratios between successive eigenvalues, E_{i-1}/E_i. The PCA routine performs analysis on standardized variables, meaning that they are rescaled to have a zero mean and unit variance. This means that the relative sizes of the eigenvalues tells something physical about the relative variance of the data in different "directions." The last column, labeled σ, shows the total variance in the input variable before it was rescaled.

We can see in Table 4 that the first two eigenvalues are comparable in size ($E_1/E_2 = 1.3$) and about twice as large as the third, after which there are five vectors of comparable size (with ratios of ~1.0–1.3), until the last two values which are smaller again. In physical terms, this can be interpreted as the variance in the data being slightly larger in two directions, then of comparable size until we have two directions which have quite small variance. There is not one *much* stronger trend between variables than any other. From the size of the components on the first eigenvector, we see that the strongest trend is between the projected radius ($\log(r_p/r_e)$) and the local surface brightness, μ_z (since these have the largest components of the first eigenvector). The next strongest trend (two largest projections onto V2) is between the galaxy color and average surface brightness.

Obviously μ_z and r_p/r_e are related through the surface brightness profile of the galaxy, and therefore a relatively strong trend between them is expected. Since these trace almost the same physical property (i.e., the local environment of the GCs), we chose to drop r_p/r_e in further analysis (this choice is also discussed in Section 5).

Running PCA on the remaining seven environmental factors and the half-light radius shows that the strongest residual correlations are between $M_{B,\rm gal}$ and the color of the galaxy. We argue below that $M_{B,\rm gal}$ and $(g-z)_{\rm gal}$ are providing complementary information about the host galaxy (because of the well-known color–magnitude relation in early-type galaxies), and therefore chose to keep galaxy color as a distance independent variable. We will also drop the GC magnitude z at this point as the last remaining distance dependent factor.

Running the PCA on the remaining five environmental factors, we then find a distribution which shows a relatively strong trend between the galaxy color and surface brightness (both local and global), and weaker trends between the rest of the variables. The half-light radius ($\log(r_h)$) is most strongly projected onto the third eigenvector along with (in decreasing order) the color at the position of the GC ($\mu_g - \mu_z$) and the surface brightness at position of the GC (μ_z)—both tracers of the local environment of the GC. The full numeric outcome is shown in Table 5.

We run two final PCAs on a set of three environmental factors plus the GC half-light radius—one in which the global and local

[14] http://idlastro.gsfc.nasa.gov/

Table 4
PCA Results for Input of All Eight Environmental Factors

Factor	V1	V2	V3	V4	V5	V6	V7	V8	V9	σ
$\log r_h$	0.15 ± 0.02	0.18 ± 0.02	0.69 ± 0.03	0.17 ± 0.08	0.40 ± 0.11	0.47 ± 0.10	0.13 ± 0.05	0.07 ± 0.02	0.02 ± 0.01	0.157
$(g-z)_{\rm GC}$	−0.29 ± 0.02	−0.27 ± 0.02	−0.29 ± 0.05	−0.25 ± 0.11	−0.11 ± 0.18	0.72 ± 0.11	0.29 ± 0.07	−0.16 ± 0.02	0.03 ± 0.01	0.231
$z_{\rm GC}$	0.13 ± 0.02	0.12 ± 0.02	−0.49 ± 0.10	0.68 ± 0.33	0.18 ± 0.09	0.26 ± 0.07	−0.17 ± 0.05	−0.01 ± 0.01	−0.01 ± 0.01	0.794
$\log(r_p/r_e)$	0.56 ± 0.01	−0.21 ± 0.03	0.05 ± 0.02	−0.07 ± 0.04	−0.23 ± 0.05	0.14 ± 0.07	−0.17 ± 0.03	−0.15 ± 0.01	−0.71 ± 0.01	0.384
μ_z at r_p	0.53 ± 0.01	0.05 ± 0.03	−0.10 ± 0.04	−0.28 ± 0.12	−0.08 ± 0.07	0.21 ± 0.05	−0.42 ± 0.07	0.10 ± 0.02	0.59 ± 0.01	1.657
$\mu_g-\mu_z$	0.25 ± 0.02	−0.25 ± 0.02	−0.29 ± 0.06	−0.26 ± 0.12	0.75 ± 0.13	−0.16 ± 0.19	0.20 ± 0.06	−0.13 ± 0.01	−0.04 ± 0.01	1.413
$M_{B,\rm gal}$	0.40 ± 0.01	0.29 ± 0.02	−0.17 ± 0.02	0.00 ± 0.04	−0.22 ± 0.05	−0.04 ± 0.08	0.71 ± 0.11	0.39 ± 0.02	0.03 ± 0.01	1.373
$(g-z)_{\rm gal}$	−0.06 ± 0.03	−0.64 ± 0.01	0.06 ± 0.02	0.12 ± 0.05	0.03 ± 0.02	0.01 ± 0.02	−0.08 ± 0.02	0.74 ± 0.01	−0.00 ± 0.01	0.092
$\langle\mu_z\rangle$	−0.22 ± 0.03	0.52 ± 0.02	−0.22 ± 0.05	−0.32 ± 0.13	0.20 ± 0.05	0.15 ± 0.06	−0.29 ± 0.05	0.47 ± 0.01	−0.38 ± 0.01	0.927
E-values (%)	28.0 ± 0.3	21.6 ± 0.4	12.0 ± 0.2	10.7 ± 0.2	9.0 ± 0.2	8.2 ± 0.2	6.5 ± 0.2	3.3 ± 0.1	0.7 ± 0.1	
E_{i-1}/E_i		1.3	1.8	1.1	1.2	1.1	1.3	2.0	4.8	

Table 5
PCA Results for Input of Reduced Set of Five Environmental Factors

Factor	V1	V2	V3	V4	V5	V6	σ
$\log r_h$	0.27 ± 0.03	0.29 ± 0.04	0.62 ± 0.04	0.66 ± 0.03	0.08 ± 0.05	0.06 ± 0.02	0.157
$(g-z)_{GC}$	−0.34 ± 0.03	−0.45 ± 0.03	−0.26 ± 0.03	0.64 ± 0.03	−0.24 ± 0.23	−0.28 ± 0.02	0.231
μ_z at r_p	0.16 ± 0.05	0.59 ± 0.02	−0.35 ± 0.03	0.06 ± 0.06	−0.54 ± 0.43	0.12 ± 0.02	1.657
$\mu_g - \mu_z$	−0.25 ± 0.05	0.49 ± 0.03	−0.48 ± 0.03	0.28 ± 0.06	0.48 ± 0.37	−0.12 ± 0.02	1.413
$(g-z)_{gal}$	−0.67 ± 0.01	0.05 ± 0.05	0.17 ± 0.02	0.03 ± 0.02	−0.05 ± 0.05	0.72 ± 0.01	0.092
$\langle\mu_z\rangle$	0.52 ± 0.02	−0.33 ± 0.04	−0.40 ± 0.02	0.24 ± 0.03	0.14 ± 0.10	0.61 ± 0.01	1.199
E-values (%)	29.3 ± 0.5	24.8 ± 0.4	17.0 ± 0.4	12.8 ± 0.3	10.3 ± 0.3	5.8 ± 0.2	
E_{i-1}/E_i		1.2	1.5	1.3	1.2	1.8	

Table 6
PCA Results for Input of First Reduced Set of Three Environmental Factors—Using Colors

Factor	V1	V2	V3	V4	σ
$\log r_h$	0.49 ± 0.02	0.28 ± 0.06	0.81 ± 0.02	0.14 ± 0.05	0.158
$(g-z)_{GC}$	−0.56 ± 0.02	−0.40 ± 0.04	0.37 ± 0.04	0.61 ± 0.09	0.231
$\mu_g - \mu_z$ at r_p	−0.27 ± 0.04	0.84 ± 0.02	−0.20 ± 0.06	0.42 ± 0.07	1.657
$(g-z)_{gal}$	−0.61 ± 0.01	0.22 ± 0.03	0.39 ± 0.05	−0.64 ± 0.10	0.092
E-values (%)	37.0 ± 0.6	26.3 ± 0.4	20.8 ± 0.4	15.9 ± 0.4	
E_{i-1}/E_i		1.4	1.3	1.3	

Table 7
PCA Results for Input of Second Reduced Set of Three Environmental Factors—Using Surface Brightness

Factor	V1	V2	V3	V4	σ
$\log r_h$	−0.50 ± 0.13	−0.20 ± 0.10	−0.52 ± 0.52	−0.25 ± 0.30	0.158
$(g-z)_{GC}$	0.62 ± 0.16	0.06 ± 0.05	−0.05 ± 0.07	−0.50 ± 0.58	0.231
μ_z at r_p	−0.54 ± 0.14	0.03 ± 0.09	0.46 ± 0.45	−0.34 ± 0.39	1.657
$\langle\mu_z\rangle$	0.13 ± 0.05	−0.96 ± 0.12	0.16 ± 0.13	0.01 ± 0.06	0.927
E-values (%)	35.0 ± 0.5	25.0 ± 0.2	22.0 ± 0.4	18.1 ± 0.4	
E_{i-1}/E_i		1.4	1.1	1.2	

environment properties are described by surface brightness, and another using the global and local colors. These final PCAs on a limited set of parameters now indicate a roughly "spherical" distribution of points, in both of these four-dimensional spaces (see numerical results in Tables 6 and 7). This indicates that there is no one trend between parameters which is significantly stronger than any other. It also seems to not matter if we use the surface brightness or color to trace of the global and local properties of the host galaxy.

The scaling relation between variables X and Y can be found from the primary eigenvector, rescaled by the standard deviations of X and Y as

$$X \propto \frac{V_1(Y)/\sigma_Y}{V_1(X)/\sigma_X} Y. \quad \text{(A1)}$$

We do not expect to find exactly the same scaling relations of $\log r_h$ here as we will when we consider the 2D trends since in the 2D trends we attempt to find a representative fit not simply dominated by the massive galaxies with large numbers of GCs (and generally at smaller radii compared to r_e because of the size of the ACS field). For example, below, we often fit the trends in each galaxy separately, then make averages of all the trends in all the galaxies. We also consider blue and red GCs separately (although we find no significant differences), and consider the trend of $\log r_h$ with GC color only after the corrections for local and global factors are made. All of this is explained in greater detail in Section 5 but is included here to explain why we do not place weight on the scaling relations found from the PCA, but rather use it only as a way to make sure we are not missing any unexpected correlations and have included all the important factors.

The final conclusion from our PCA here is that the variability in the values of r_h of GCs can be described reasonably well using three factors, one each from the internal, local, and global properties (as defined in Section 4).

REFERENCES

Aarseth, S. J., & Heggie, D. C. 1998, MNRAS, 297, 794
Barmby, P., McLaughlin, D. E., Harris, W. E., Harris, G. L. H., & Forbes, D. A. 2007, AJ, 133, 2764
Blakeslee, J. P., et al. 2009, ApJ, 694, 556
Côté, P., et al. 2004, ApJS, 153, 223
Da Costa, G. S., Grebel, E. K., Jerjen, H., Rejkuba, M., & Sharina, M. E. 2009, AJ, 137, 4361
DeGraaff, R. B., Blakeslee, J. P., Meurer, G. R., & Putman, M. E. 2007, ApJ, 671, 1624
de Vaucouleurs, G., de Vaucouleurs, A., Corwin, H. G., Buta, R. J., Paturel, G., & Fouqué, P. 1991, Third Reference Catalogue of Bright Galaxies (New York: Springer)
Ferguson, H. C. 1989, AJ, 98, 367
Ferrarese, L., et al. 2006, ApJS, 164, 334
Forbes, D. A., Masters, K. L., Minniti, D., & Barmby, P. 2000, A&A, 358, 471
Forbes, D. A., Spitler, L. R., Harris, W. E., Bailin, J., Strader, J., Brodie, J. P., & Larsen, S. S. 2010, MNRAS, 403, 429
Georgiev, I. Y., Puzia, T. H., Hilker, M., & Goudfrooij, P. 2009, MNRAS, 392, 879
Gómez, M., & Woodley, K. A. 2007, ApJ, 670, L105
Goudfrooij, P., Alonso, M. V., Maraston, C., & Minniti, D. 2001, MNRAS, 328, 237

Harris, W. E. 2009, ApJ, 699, 254
Harris, W. E., Mouhcine, M., Rejkuba, M., & Ibata, R. 2009a, MNRAS, 395, 436
Harris, W. E., Spitler, L. R., Forbes, D. A., & Bailin, J. 2009b, MNRAS, 401, 1965
Haşegan, M., et al. 2005, ApJ, 627, 203
Jordán, A. 2004, ApJ, 613, L117
Jordán, A., et al. 2005, ApJ, 634, 1002 (J05)
Jordán, A., et al. 2007a, ApJS, 169, 213
Jordán, A., et al. 2007b, ApJS, 171, 101
Jordán, A., et al. 2009, ApJS, 180, 54
Kundu, A., & Whitmore, B. C. 2001, AJ, 121, 2950
Kundu, A., Whitmore, B. C., Sparks, W. B., Macchetto, F. D., Zepf, S. E., & Ashman, K. M. 1999, ApJ, 513, 733
Larsen, S. S., & Brodie, J. 2003, ApJ, 593, 340
Larsen, S. S., Brodie, J. P., Huchra, J. P., Forbes, D. A., & Grillmair, C. 2001, AJ, 121, 2974
Lightman, A. P., & Shapiro, S. L. 1978, Rev. Mod. Phys., 50, 437
Madrid, J. P., Harris, W. E., Blakeslee, J. P., & Gómez, M. 2009, ApJ, 705, 237
McLaughlin, D. E. 2000, ApJ, 539, 618
McLaughlin, D. E., Barmby, P., Harris, W. E., Forbes, D. A., & Harris, G. L. H. 2008, MNRAS, 384, 563
McLaughlin, D. E., & Pudritz, R. E. 1996, ApJ, 469, 194
Mei, S., et al. 2007, ApJ, 655, 144
Murphy, B. W., Cohn, H. N., & Hut, P. 1990, MNRAS, 245, 335
Murray, N. 2009, ApJ, 691, 946
Murray, S. D., & Lin, D. N. C. 1992, ApJ, 400, 265
Murtagh, F., & Heck, A. (ed.) 1987, Multivariate Data Analysis (Dordrecht: Reidel), 33
Peng, E. W., et al. 2006, ApJ, 639, 95
Peng, E. W., et al. 2009, ApJ, 703, 42
Puzia, T. H., Kissler-Patig, M., Brodie, J. P., & Huchra, J. P. 1999, AJ, 118, 2734
Schweizer, F. 1980, ApJ, 237, 303
Shapley, H., & Sawyer, H. B. 1927, Harv. Coll. Obs. Bull., 852, 22
Spitler, L. R., Larsen, S. S., Strader, J., Brodie, J. P., Forbes, D. A., & Beasley, M. A. 2006, AJ, 132, 1593
Spitzer, L. J., & Thuan, T. X. 1972, ApJ, 175, 31
Woo, J., Courteau, S., & Dekel, A. 2008, MNRAS, 390, 1453